Chapter 10
Applications of the Inverse Problem of Pollution Propagation

Tarmo Soomere

Abstract The quantification of the potential of different offshore domains to serve as a remote source of danger to the vulnerable areas through pollution propagation is developed into a technique for the environmental management of open sea regions. The technique focuses on the identification of areas (of reduced risk) that provide the lowest level of environmental concerns for offshore activities. An approximate solution to the relevant inverse problem is constructed by means of statistical analysis of a large number of Lagrangian trajectories of pollution particles. The method contains an eddy-resolving circulation model, a scheme for the tracking of Lagrangian trajectories, a technique for the calculation of quantities characterizing the potential of different sea areas to supply adverse impacts, and routines to construct the optimum fairway. The distributions of the probability of current-driven transport of pollution to vulnerable domains and its propagation time are used for the optimization of the location of potentially dangerous activities. This technique is applied for the optimization of marine fairways to minimize the risk to high-value areas in two regions of the Baltic Sea. The environmental advantage is expressed in terms of the probability of pollution transport to the nearshore and the associated time (particle age). In the Gulf of Finland the use of the optimum fairway would decrease the probability of coastal pollution by 40 % or increase the average time it takes for the pollution to reach the coast from 5.3 to about 9 days.

10.1 Introduction

Modelling efforts addressing the transport of oil spills (or any other adverse impacts such as chemical pollution, or items on the sea surface such as lost containers, rescue boats, ships without propulsion, etc.) mostly focus on the direct problem of

T. Soomere (✉)
Wave Engineering Laboratory, Institute of Cybernetics at Tallinn University of Technology, Akadeemia tee 21, 12618 Tallinn, Estonia
e-mail: tarmo.soomere@cs.ioc.ee

T. Soomere
Estonian Academy of Sciences, Kohtu 6, 10130 Tallinn, Estonia

T. Soomere, E. Quak (eds.), *Preventive Methods for Coastal Protection*,
DOI 10.1007/978-3-319-00440-2_10,

pollution propagation in the marine environment. The forecast is usually provided for the given location of the source, the amount and the properties of the spilled oil, and modelled metocean conditions (e.g., French et al. 1997; Reed et al. 1999; French-McCay 2004; Ambjörn 2008). The results definitely assist in taking countermeasures after an oil spill has occurred. The systematic use of the Lagrangian approach makes it possible to estimate the probability of a region to be polluted, the time it takes for the oil to reach a specific site, and the areas that could be a threat for a given shoreline (Abascal et al. 2010). Sometimes backwards tracking of the drift allows the origin of the spill to be determined and to catch the guilty party (Ambjörn 2008).

10.1.1 The Hidden Potential of Currents

The technique described in this chapter goes one step further. The goal is to establish for which release sites an oil spill will cause the least damage under the same hydrometeorological conditions and to develop examples of engineering solutions for optimizing some important activities accordingly.

Since the drift of oil is also affected by direct wind drag and wave-driven impact, its adequate description generally presumes that these factors are considered. The transport induced by wind drag and wave motion is mostly 'downwind' or 'downwave', respectively, and the odds for an area to be affected are roughly inversely proportional to its distance from the pollution release site in those directions. The regions associated with the lowest risk are thus as far 'upwind/upwave' from the vulnerable location as possible. As the impact of wind and waves can be relatively easily added to the model, the presentation here is limited to the quantification of the current-driven transport. An example of the combined analysis of current-, wind- and wave-driven transport is presented in Chap. 11.

The current-driven transport has the largest unused potential for the reduction of coastal pollution. A pattern of currents is an integral reaction of water masses to a variety of forcing factors. It is usually highly complicated even if the wind is stationary. The currents are often directed against wave-induced transport or wind drag (e.g., Andrejev et al. 2004a; Gästgifvars et al. 2006). The forecast of current-induced transport of drifters is only reliable within about 0.5 days (Vandenbulcke et al. 2009). Even small errors in the initial location of drifters can drastically change the calculated trajectories (Griffa et al. 2004).

A necessary prerequisite for undertaking a systematic search for an optimum release site is the presence of nontrivial, anisotropic internal dynamics of surface currents: otherwise different release sites can simply be graded according to their distance from the vulnerable spots. The anisotropy of transport patterns intrinsically characterizes jet-like currents but has also been shown to hold for sea areas with seemingly highly random dynamics such as the Baltic Sea (Meier 2007; Lu et al. 2012). Although trajectories of water particles may be extremely complicated (see Fig. 9.6 in Chap. 9), they are never completely random. For example,

the net current-driven transport frequently has semi-persistent patterns on the surface (Soomere et al. 2011d; Lu et al. 2012) or in the subsurface layer (Andrejev et al. 2004a, 2004b). These usually concealed patterns make the probability of transport of various substances between different sea areas highly variable. The resulting current-driven transport may be at times directed across relatively narrow regions (Soomere et al. 2011d) and/or may lead to unexpectedly high probability of transport of adverse impacts between certain regions (Lekien et al. 2003). The challenge addressed here is how to quantify the impact of this transport in some commonly usable and clearly understandable categories.

10.1.2 The Value of Different Sea Areas

This challenge is only meaningful if some value is assigned to certain regions. The difference in the value of various offshore and nearshore domains was recognized many centuries ago (Bowden-Kerby 2001). It is legally formulated in the recent past through establishing marine protected areas and developing the concept of particularly sensitive sea areas (Kachel 2008). Giving some regions a certain value naturally generates a spatio-temporal distribution of costs of consequences. Namely, similar accidents but occurring at different locations usually impact the valuable areas differently.

This distribution obviously depends on the demarcation of the valuable areas and on the assigned 'price.' For some cases (e.g., the collision with a whale, Stokstad 2009) the cost is evident immediately at the site and the use of its spatial distribution (e.g., the frequency of observations of the whales) for environmental management is straightforward. Still on many occasions a substantial part of the costs becomes evident later through some hidden or hardly predictable mechanism of remote impact. Some of these situations (e.g., the propagation of an ash cloud after a volcano eruption) are out of the control of society. Many others (incl. ship accidents), however, allow at least limited human control.

A generic example of a dangerous event with substantial remote impact, used in this book to illustrate the developed technique, is an oil spill. It is obviously undesirable everywhere on the sea but the scale of the associated devastation drastically increases when it drifts to some valuable area. It is not possible to control the wind, waves or currents that govern the fate of an oil spill but it is viable to restrict, at least to some extent, the location of the potential sources of oil spills.

If vulnerable spots are selected based on environmental criteria a smart use of the factors that drive the oil propagation may provide a natural way to mitigate the environmental damage. This chapter presents a technique for applying knowledge of natural processes for this purpose and provides several examples about how to use it for decision-making. An important step is the identification of areas of reduced risk, so that for accidents occurring there, the costs through current-driven remote impact are lower than for adjacent areas. In many cases directing activities to these areas involves marginal additional costs. A corresponding policy may serve

as a qualitatively new way of protecting vulnerable areas (Soomere and Quak 2007; Soomere et al. 2010).

There exist an enormous variety of ecological values and indicators of environmental well-being (Rice 2003). Using oil pollution as an example of a dangerous event, it is natural to treat the pollution of the nearshore (called a *coastal hit* below), wherever it happens, as a highly undesired and costly consequence. This setting underlines the importance of coastal domains in the marine ecosystem according to the common opinion that shallow-water and nearshore areas frequently have the largest ecological and environmental value (Gray 1997; Kokkonen et al. 2010). Like any other assignment of values, it obviously generates an associated distribution of costs of otherwise similar accidents occurring at different sites.

10.1.3 The Inverse Problem

The practical use of this idea generally requires solving an inverse problem of the identification of the most favourable location for the oil release. Its straightforward solution presumes inverse tracking of pollution propagation, similar to the problem of establishing the origin of illegal oil spills. The methods for effectively solving inverse problems are considerably less developed than those used for direct problems. Although many trajectory-tracking (such as TRACMASS described in Chap. 7) and oil drift models (e.g., Ambjörn 2007) are formally invertible, such problems are frequently mathematically ill-posed. A straightforward solution to these is not possible and no universal method exists for their analysis.

The determination of the offshore domains that systematically offer the least danger to the environment in terms of the transport of various adverse impacts to vulnerable regions owing to different hydrometeorological factors is an extension of the problem of the analysis of current-induced Lagrangian transport addressed in the previous chapter. It is natural to use the same technique—statistical analysis of a large pool of examples of current-driven pollution propagation—for solving it.

The variety of different environmental values naturally generates a similar variety of meaningful ways to characterize the ‘damage potential’ of the offshore areas. They may be quantified, for example, according to the probability of pollution released in these areas to reach vulnerable regions, or in terms of time it takes for this impact to reach the coast after an accident has happened. For any measure in use, the goal is to identify the areas that offer the least ‘cost’ of accidents. As discussed in Chap. 1, doing so is one of the two possible ways to reduce environmental risks associated with this particular type of damage. For example, in terms of probabilities those domains are preferable, from which the propagation of adverse impacts to high-value areas is most unlikely. The resulting quantification makes it possible to find optimum locations of oil platforms, or where to tow a leaking vessel, among a set of technically feasible solutions.

A highly interesting application is the specification of optimum fairways for semi-enclosed seas. Such sailing lines offer a reduced level of remote impact of ship

traffic on the environment in a fairly general framework that accounts not only for the local costs of accidents but also reveals the costs that become evident later, far from the accident site through the propagation of various adverse impacts released either occasionally or as a consequence of an accident. This concept is a generalization of the idea of applying emerging knowledge about semi-persistent current patterns to minimize the consequences of potential accidents (e.g., by routing ship traffic through specific areas, Soomere and Quak 2007). A decrease in the aggregate environmental risk (see Eq. (1.1) in Chap. 1) is achieved preventively, before the accident happens. Similar applications can also be developed to specify how far from the open ocean coast an economically feasible and environmentally friendly sailing line should be located (Soomere et al. 2011c).

10.2 The Use of Lagrangian Trajectories of Current-Driven Transport in the Surface Layer

The problem of identifying the least dangerous offshore areas can be simplified by considering an oil spill as a cluster of persistent oil particles of neutral buoyancy that are passively carried with surface currents. Then an approximate quantification of the level of danger posed by oil spills can be obtained by the statistical analysis of a large number of Lagrangian trajectories of single pollution particles released to the sea at different time instants and locations (Abascal et al. 2010; Soomere et al. 2010). An approximation of the areas of reduced risk is thus sought through the extraction of information from a large pool of particular solutions of the direct problem of propagation of oil particles.

The previous chapter demonstrated the potential of this approach to unveil the presence of very rich, usually concealed internal structures of semi-persistent transport patterns in certain sea areas (Soomere et al. 2011d). This chapter focuses on a subset of such patterns that may bring oil pollution close to the coast. The major technical problems are the same: (i) how to extract useful information from the vast amount of numerically simulated data, and (ii) how to realize an implementation for the shipping or offshore industry based on the extracted information.

For simplicity, the potential of the technique is demonstrated here for the particular case when the trajectories of particles representing adverse impacts are locked in the uppermost layer and thus reflect the behaviour of the lighter fractions of the oil pollution. Although we only consider a few examples of simplified environmental criteriaenvironmental criterion, the approach can be easily modified to account for virtually any realistic set of measures or to be used in combination with practically any set of values of different areas uniquely defined in time and space. The resulting engineering solutions (e.g., an optimum fairway) of course depend on the particular choice of the measures and values.

10.2.1 Quantification of Environmental Risks

A commonly used measure is the probability of the valuable areas being hit by pollution. It is straightforward to associate with each offshore point the probability of oil propagation from this site to a certain vulnerable area. Its sensible use implicitly requires the setting of a (propagation) time scale over which this probability is counted (Andrejev et al. 2010; Viikmäe et al. 2010). Doing so naturally leads to a complementary quantity that can equally well characterize the potential of pollution released at a particular sea point to pose danger to the nearshore: the average time it takes for the pollution to reach the valuable area. This measure is similar to commonly used water age (Deleersnijder et al. 2001) and is called particle age in the following discussion. It naturally characterizes the cost of consequences from another viewpoint: the longer time pollution remains in the open sea, the larger fraction of it will be weathered or may be removed before it hits a vulnerable spot.

These measures are of course not equivalent. The values of particle age intrinsically contain information about whether the particle had reached the vulnerable area. A hit to a valuable area obviously has occurred if the age of a particle is less than the propagation time. Therefore it is straightforward to evaluate the probability of hits to the vulnerable areas once the values of the age of all particles are known. An inversion of this operation is not possible because the values of probability only contain information about whether or not a hit has occurred.

The quantification is performed in this chapter in the context of the propagation of oil pollution from different offshore areas to the nearshore. It is obviously applicable for any adverse impact that is passively carried by surface currents. Its possibilities are demonstrated for relatively simple particular cases of constant-value coast. These examples are rich enough in content to highlight not only the complexity of the problem but also the variety of solutions depending on a particular set-up and intrinsic uncertainties of the technology. Accounting for the more complicated internal structure of the high-value areas is also straightforward. For example, it is possible to identify certain locations from where the oil is less likely to be transported to selected vulnerable spots of any kind (e.g., marine protected areas, Delpeche-Ellmann and Soomere 2013), or from where the transport will take a longer time (Viikmäe and Soomere 2013).

10.2.2 Preventive Optimization of Dangerous Activities

Once a map of the probabilities of hitting a specific area (or particle age) has been constructed, the optimum locations for potentially dangerous activities (areas of reduced risk) are the minima for the probabilities or the maxima for the particle age. The obvious practical outcome is the possibility to plan (or redirect) dangerous activities into such areas. These maps are, however, of much larger practical importance. They may serve as the basis for various engineering solutions, decision support systems and preventive methods for the environmental management of shipping

and offshore activities by means of optimization of the location of potential release of adverse impacts.

An important application is their use for optimizing fairways in domains (such as the North Sea or Baltic Sea and especially the narrow and shallow Gulf of Finland) that host extremely heavy ship traffic in the immediate neighbourhood of valuable areas or sectors of the coast. In this context, the formulated problem is equivalent to the task of minimizing the environmental damage for a moving source of danger. It can be naturally associated with the classical problem of smart ship routing once the distribution of the underlying quantities is known. For example, an approximate solution for the environmentally safest sailing line is to route the ships along the minima of these probabilities (Andrejev et al. 2011).

Alternatively, one can benefit from a choice of the sailing line for a (chemical) tanker that provides a systematic increase in the time it takes before the adverse impact reaches a vulnerable area (Engqvist and Andrejev 2003; Engqvist et al. 2006). The use of the maxima for the particle age (Andrejev et al. 2011) for this purpose is equivalent to buying extra time to combat the leak while the spill travels to the coast.

For elongated sea areas (such as the Gulf of Finland), it might also rational to search for the *equiprobability line*, such that for each of its points it is equally probable that the spill reaches one coastline or the opposite one during a certain time interval (Soomere et al. 2010). A further challenge (addressed only partially below) is to minimize the cost of damage so that the additional economic costs would remain manageable.

The goal of this technique is not to produce yet another operational model to assist rescue and oil combating teams after an accident has happened. Instead the goal is to identify beforehand the regions where it is statistically safer to travel. The target is thus the preventive reduction of environmental risks: an optimization of the location of potentially dangerous activities (e.g., ship traffic) so that the consequences of the resulting unfortunate event (here in terms of the impact of substances potentially released into the sea and transported by currents) upon high-cost areas would be minimal once it indeed occurred (cf. Eide et al. 2007).

A precondition for the use of such a way of thinking is the heterogeneity of the relevant physical or ecological fields (such as the resulting maps of the probabilities of coastal hit or the particle age). A recent solution of this kind is the relocation of the fairway entering Boston Harbour (Massachusetts, USA) to minimize the probability of collisions of ship traffic with globally endangered right whales (Stokstad 2009). This action was based on the existence of an area, which was only infrequently visited by whales and thus offered a clear decrease in the probability for a collision.

10.3 Components of the Technique and Properties of Test Areas

The technology contains four basic steps (Soomere et al. 2011a). The basis is a high-resolution three-dimensional (3D) ocean circulation model. As a prerequisite, the

model is supposed to adequately resolve the current-driven transport in the area in question and to provide (numerically simulated Eulerian) velocities at certain grid points and with a certain temporal resolution over a long time period. Secondly, the generated velocity data are used to compute Lagrangian trajectories of a large number of water particles. These particles are interpreted as passive tracers representing potentially adverse substances of neutral buoyancy (e.g., single oil particles) released at different locations and at different time instants.

Thirdly, the trajectories are analysed with respect to a given cost function and/or problem setup using standard statistical methods. This analysis leads to a spatial quantification of the offshore areas. Note that the resulting distributions characterize the points of release of adverse impacts rather than the vulnerable areas. Finally, the spatial distributions of these quantities (optionally together with additional constraints such as the location of the ports) are used for decision-making, for example, for the identification of the optimum location of the fairways, by choosing them as close as possible to the local or global minima of the distributions.

Each of the steps requires a number of parameters, implicit time scales and options that may potentially affect the resulting 2D distributions (maps) and the further decision-making process. The existing implementations have applied the steps consecutively. This made it possible to improve the particular methods used within steps separately (Andrejev et al. 2010; Viikmäe et al. 2010). Some relevant issues are discussed in Chap. 9 and in Viikmäe et al. (2010). The dependence of the results on the choice of the options was evident in the early analysis (Soomere et al. 2010) where the equiprobability lines were calculated using two slightly different sets of trajectories. The optimum fairways also depend substantially on the resolution of the ocean model (Andrejev et al. 2010). The strong seasonal variation of net and bulk transport patterns (Chap. 9; Soomere et al. 2011d) suggests that seasonally optimum fairways may be radically different for windy and calm seasons in the Gulf of Finland as also discussed in Chap. 11. Lu et al. (2012) showed that extensive variations in the optimum fairway correspond to the inflow and outflow situations in the south-western (SW) Baltic Sea.

10.3.1 The Baltic Sea Under Pressure

There are several reasons why this technique has been first implemented for the Baltic Sea (Fig. 10.1). This water body is under strong pressure from shipping and other offshore activities. The concentration of ship traffic (including tankers of various kinds) is exceptionally high (HELCOM 2009). More than 70 large ports handle more than 1 million tonnes of cargo per year. The number of ship voyages (excluding ferry traffic) is estimated at 150,000 per year (Gollasch and Leppäkoski 2007), and it is assumed that it will increase considerably in the future. Since 1980 the Baltic Sea has experienced on average one major shipping accident per year resulting in an oil spill larger than 100 tonnes (WWF 2010).

Fig. 10.1 Baltic Sea and the test regions in the Gulf of Finland and the SW Baltic Sea and the Danish Straits. Graphics by M. Viška

The sea has been used for dumping massive quantities of waste, explosives and extremely dangerous chemical warfare agents (Glasby 1997). Currently it hosts several large-scale controversial constructions (Lidskog and Elander 2012) and a few oil platforms (WWF 2010). The number of offshore installations may soon increase considerably through ambitious plans for the erection of wind parks that might fill large sections of the offshore with sizeable structures and cables. The resulting high probability of the release of various undesirable substances into the sea as a result of an accident, a technical problem, human error or deliberate action is alarming because the consequences of a major pollution event could be devastating for this particularly sensitive sea area (Kachel 2008).

The Baltic Sea is one of the most studied domains of the ocean. Many data sets extend back more than two centuries (Leppäranta and Myrberg 2009). Reliable and thoroughly validated atmospheric and ocean models exist for this region (Meier et al. 2003; Myrberg et al. 2010b). Its mesoscale dynamics has a complexity comparable with that of the open ocean. The sea is known to have numerous semi-persistent patterns of both surface and subsurface currents (Lehmann et al. 2002; Andrejev et al. 2004a, 2004b; Meier 2007; Osiński and Piechura 2009; Soomere et al. 2010).

The technology described here has been applied at a moderate resolution for the entire Baltic Sea and at a higher resolution for two test areas, the SW Baltic Sea and the Gulf of Finland. An other version based on Eulerian tracking of pollution propagation (Höglund and Meier 2012) described in Chap. 4 has also been applied

to the entire Baltic Sea. The test areas not only play a key role in the functioning of the sea (as described in Chaps. 2 and 6) but also exhibit different challenges for the technique.

10.3.2 The Western and Eastern Gateways to the Baltic Sea

The Danish Straits, the Belt Sea and the Arkona Basin form the gateway through which all the ships travelling between the North Sea and the Baltic Sea have to pass (see Figs. 9.1 and 9.2 in Chap. 9). This mostly shallow domain with moderately sloping bottom serves as a transit area for the outflow of excess water through the Danish Straits. More importantly, it is the gate through which the deeper parts of the Baltic Sea are sporadically supplied under specific atmospheric conditions with saltier, oxygen-rich North Sea waters (Matthäus and Lass 1995).

The complicated geometry of the coasts, the presence of narrow straits and the small internal (baroclinic) Rossby radius R_1 (about 5 km in the Arkona Basin and the Pomeranian Bay, Osiński et al. 2010, and as small as 1–4 km in the shallow Belt Sea, Fennel et al. 1991) make numerical modelling of water masses extremely challenging. In order to properly resolve mesoscale dynamics, it is necessary to use a horizontal grid size not larger than about $1/2$ of the baroclinic Rossby radius (Drijfhout 1989; Lindow 1997). Most medium-resolution Baltic Sea circulation models have a grid step around 2 nautical miles (nm) and are barely eddy-permitting here. Furthermore, fine vertical resolution is needed here to resolve the straits' topography and sharp stratification (Lu et al. 2012).

The Gulf of Finland (see Chap. 6) is an elongated estuary (length over 400 km, width 48–135 km) in the north-eastern (NE) Baltic Sea with a mean depth of 37 m only (Alenius et al. 1998). As it is quite narrow in some places and the water is too shallow for marine transportation in others, there are several narrow passages where the concentration of traffic is exceptionally high. Particularly intense passenger traffic crosses the narrow section of the gulf between Tallinn and Helsinki (Parnell et al. 2008; Kurennoy et al. 2011).

The gulf is widely open to the Northern Gotland Basin. As there is no sill at its entrance, continuous water exchange occurs between the two water bodies and the dynamics of the Baltic Proper[1] strongly affects currents in the western part of the gulf. This region evidently plays a key role in the functioning of the northern Baltic Sea. Under specific wind conditions the typical estuarine circulation may be reversed, the salt water wedge may be exported from the gulf and the vertical stratification may almost completely vanish (Elken et al. 2003). This process may lead to enhanced vertical mixing of water masses. The eastern end of the gulf receives voluminous fresh water inflow from the River Neva. This gives rise to a strong east–west gradient in salinity and sea-level and leads to a small baroclinic Rossby

[1] We shall use the notion Baltic Proper to denote the Eastern, Northern and Western Gotland Basin (Table 2.1 in Chap. 2), Bornholm Basin and Gdańsk Bay.

radius (usually about 2–4 km) (Alenius et al. 2003) and enhanced buoyancy-driven currents.

These features favour intricate spatio-temporal patterns in salinity and density, and support a complicated interplay of the basin-scale cyclonic circulation, the exchange of water masses with the Baltic Proper, and the system of mesoscale (synoptic) eddies (Andrejev et al. 2004a, 2004b). In addition, these patterns become even more complicated due to substantial seasonal variations in the wind field and the incoming solar radiation, and to the possible presence of an ice cover (Myrberg and Andrejev 2003; Andrejev et al. 2004a, 2004b; Myrberg et al. 2010b). Consequently, the requirements for circulation modelling for the Gulf of Finland are as high as for the SW Baltic Sea. The common circulation models with a grid step of 2–3 nm (Myrberg et al. 2010b) apparently overlook a part of its dynamics, especially the contribution by synoptic eddies to circulation and mixing.

10.4 Circulation and Trajectory Models

The quality of the circulation models is crucial for the success of the entire technology. Three different ocean models have been used to simulate the 3D dynamics of the Baltic Sea and in the test areas for the applications of the technique developed in 2009–2012 in the framework of the BONUS *BalticWay* cooperation.

10.4.1 The Rossby Centre Ocean Model RCO

A set of velocity fields was calculated by the Swedish Meteorological and Hydrological Institute using the Rossby Centre Ocean circulation model (RCO) for the entire Baltic Sea (Chap. 4). The model details, set-up and extensive validation efforts are described in a number of publications (Meier 2001, 2007; Meier et al. 2003, among others). The bathymetric information is based on the data set of Seifert et al. (2001). The RCO model is a further development of the Ocean Circulation and Climate Advanced Model (OCCAM) primitive-equation free-surface circulation model (based on the Bryan–Cox–Semtner model, Webb et al. 1997) in z-coordinates. It covers the entire Baltic Sea with a horizontal resolution of 2 nm and vertical resolution from 3 m in the uppermost layer down to 12 m in the deeper areas (for a total of 41 levels). This horizontal resolution is usually sufficient for eddy-resolving runs in the Baltic Proper (Lehmann 1995) but is barely eddy-permitting in the Gulf of Finland (cf. Albretsen and Røed 2010).

The model contains several parameterizations with a special importance for the Baltic Sea, such as a two-equation turbulence closure scheme of the k–ε type to parameterize subgrid-scale mixing, open boundary conditions in the northern Kattegat (in the sea area to the west of southern Sweden in Fig. 10.1), a sea-ice model and a parameterization of the effect of breaking surface gravity waves. The time-splitting

is used with the time step of 150 s for the baroclinic and 15 s for the barotropic propagation. The output is stored once in six hours to keep the size of output information at a reasonable level.

The RCO model was forced with meteorological data from a regionalization of the ERA-40 reanalysis over Europe using a regional atmosphere model covering the Baltic Sea with a horizontal resolution of 25 km during 1961–2007 (Samuelsson et al. 2011). This data set contains wind at the 10 m level (adjusted using simulated gustiness, Höglund et al. 2009), air temperature, relative and specific humidity at the 2 m level, total precipitation and total cloudiness with a temporal resolution of 3 hours, sea level atmospheric pressure, snow depth, actual albedo, short- and long-wave radiation and evaporation.

10.4.2 The OAAS Model

The numerical model OAAS, constructed for use in basins with complicated bathymetry and hydrography (Andrejev and Sokolov 1989, 1990) and named after the authors (Oleg Andrejev ja Alexander Sokolov), was used to simulate the currents in the Gulf of Finland to the east of 23°27′ E. This free-surface, 3D baroclinic z-coordinate circulation model employs standard simplifications such as the Boussinesq and hydrostatic approximation, and the no-slip condition for the entire seabed. It is based on the primitive equations of horizontal momentum balance, the continuity equation and equations for the transport of heat and salt in Cartesian coordinates.

Some of the model features (such as the equation of state) have been tuned for the Baltic Sea conditions (Millero and Kremling 1976). The use of the governing equations in the flux form allows automatic maintaining of a number of integral constraints (Blumberg and Mellor 1987). The finite-difference method uses the Arakawa C-grid (Mesinger and Arakawa 1976) and the method of splitting the time step (Liu and Leendertse 1978). An overview of the model equations and the methods for their solving is presented in Andrejev and Sokolov (1989, 1990), Sokolov et al. (1997), Andrejev et al. (2004a, 2004b, 2010).

As the winters during the period covered in simulations (1987–1991) were rather mild and the Gulf of Finland was mostly free of ice, a simple parameterization was used for ice phenomena. For water temperatures below freezing point, the wind stress was decreased by a factor of 10 in order to mimic the presence of ice. At 0 °C, the vertical heat flux was stopped as long as cooling conditions prevailed. The loss of heat during ice melting was approximated by decreasing the upward heat flux in the early spring by a factor of four until the water temperature reaches +1 °C.

The model resolution, originally restricted to 1 nm in order to match the available bathymetric information (Seifert et al. 2001), has been increased to 0.25 nm for the use of the technique in question (Andrejev et al. 2010). The model was applied in three resolutions (2 nm, 1 nm and 0.5 nm) with otherwise identical set-up. The vertical resolution was 1 m in the entire water column (except for the uppermost layer

that had a thickness of 2 m). The model has shown excellent performance in different applications, from basin-scale estimates of the upwelling features in the entire Baltic Sea (Myrberg and Andrejev 2003; Myrberg et al. 2010a), mean circulation and water age (Andrejev et al. 2004a, 2004b) and various hydrophysical features of the Gulf of Finland (Myrberg et al. 2010b) down to the small-scale reproduction of surface buoy drift (Gästgifvars et al. 2006) and test simulations using a resolution of up to 0.25 nm (Viikmäe et al. 2010).

The OAAS model setup, boundary conditions and forcing data are discussed in Andrejev et al. (2010, 2011). The model was forced with the same meteorological data as the RCO model. River discharge was approximated in the OAAS model using monthly mean values for 1970–1990 (Bergström and Carlsson 1994). As a first approximation, the salinity of river water was set to zero and its temperature equal to the ambient sea water temperature at the river mouth. This approximation (equivalent to ignoring both salinity and heat flux from the rivers) is sensible in the Baltic Sea conditions, where the river water salinity is almost zero and the difference in river and sea water temperature in shallow river mouth areas is moderate.

The modelling in the Gulf of Finland started from the resting water masses and with the sea level in equilibrium with atmospheric pressure. The initial fields (water temperature and salinity) and the boundary information (the 3D structure of the salinity and temperature and sea level information) at the entrance to the gulf (Fig. 10.1) were extracted (and optionally interpolated) from the output of the RCO model at 6-hour resolution. To smooth the potential impact of the difference in the resolution between the models, the lateral diffusivity coefficient was increased in the OAAS model towards the boundary following a sine function in a sponge layer of a width of 16 nm. The modelled fields were plausible from the very beginning of calculations. The spin-up of the surface layer dynamics took ca 1–2 weeks.

10.4.3 The DMI/BSHcmod Model

Another circulation model, DMI/BSHcmod, was applied in the studies of the dynamics in the southern Baltic Sea. This is also a 3D primitive-equation, hydrostatic, free-surface ocean model. It was developed originally by the German Federal Maritime and Hydrographic Agency (BSH) (Kleine 1994; Dick et al. 2001) and further developed by the Danish Meteorological Institute (DMI). Its version developed for the Baltic Sea conditions is now known as the HIROMB-BOOS community model (Funkquist 2001) and *inter alia* serves as the underlying circulation model of Seatrack Web, the official web-based HELCOM tool for simulation of the propagation and fate of oil pollution in the Baltic Sea (Ambjörn 2007, 2008).

In order to accurately resolve the water exchange between the Baltic Sea and North Sea through the Danish Straits, three nesting levels were applied by Lu et al. (2012) (see also Chap. 5). A 2D model with a horizontal resolution of 6 nm covering a large part of the north-eastern Atlantic provided boundary conditions for a local 3D Baltic Sea–North Sea model, with a horizontal resolution of 3 nm. A finer 3D

model with a horizontal resolution of 0.5 nm and vertical resolution of 1 m covering the transition area from Skagen to Bornholm (Fig. 10.1) was two-way nested into the above Baltic Sea–North Sea model. A detailed description of this model and its forcing and boundary conditions is presented by Lu et al. (2012). Some interesting results from this model are also described in Chap. 5.

10.4.4 Trajectory Simulations Using TRACMASS

The test elements used to evaluate the risk of coastal hit by pollution released at a particular sea point and then transported by surface currents to the nearshore were numerically simulated Lagrangian trajectories of water particles passively carried by the currents. The trajectories were locked in the uppermost layer (with a depth of 3 m in the RCO model, 2 m in the OAAS model and 1 m in the DMI/BSHcmod model) and exerted only horizontal advection. They were thus not truly Lagrangian and basically represented the motion of items persistently located in the surface layer and completely following its motion. Such items and substances are generally also affected by wind drag or wave impact. The impact of these drivers is addressed in Chap. 11. Here we only consider the current-driven advection of such items.

'Off-line' simulation of the pathways of selected particles (in which the circulation modelling was separated from the trajectory calculation, see Chap. 7) was used to build the trajectories from the output of the RCO model for the Gulf of Finland (Soomere et al. 2011c, 2011d) and the northern Baltic Proper (Viikmäe et al. 2011), and from the data of the DMI/BSHcmod model for the SW Baltic Sea (Lu et al. 2012). The trajectories were calculated with the TRACMASS code (Blanke and Raynard 1997; Döös 1995; de Vries and Döös 2001) using precomputed 3D velocity fields to reconstruct the motion of the particles. See Chap. 7 for the underlying theory and several examples of the use of this model.

The results depend to some extent on the temporal resolution of both the circulation data and the accuracy of the trajectory calculation. The resulting inaccuracies of the latter may lead to a large divergence of a few simulated trajectories from the real ones (Gräwe and Wolff 2010). Given the large number of trajectories, it is natural to assume that the potential impact of the time step of the circulation data and the trajectory reconstruction scheme on the resulting statistics is minor.

In the marine environment the particles are not only transported with the instantaneous simulated velocity in each grid cell but are also affected by local motions such as diffusive processes, small-scale turbulence, local vertical motions of water particles, etc. (so-called subgrid-scale turbulence). The latter is only partially accounted for in the circulation models and, even theoretically, cannot be adequately represented in these trajectory models that exclusively rely on precomputed velocity fields. It is only possible to replicate certain statistical features of trajectories in such models.

The version of the TRACMASS code used in the described calculations did not account for the effects of subgrid turbulence. In such cases the initially close trajectories have an overly tendency to stay close while in the real atmospheric and marine

conditions the aggregated impact of small-scale features of the motions generally tends to spread closely packed particles (Richardson 1926; Ollitrault et al. 2005). It is well known that the spreading of the resulting trajectories in studies based on this version of TRACMASS has been usually much smaller than the spreading of real drifters (Jönsson et al. 2004; Engqvist et al. 2006; Döös and Engqvist 2007; Döös et al. 2008). An implicit consequence from the lack of spreading is that the nearshore had to be defined as a 3 grid cells wide zone near the coast when the TRACMASS code was used for the Gulf of Finland (Viikmäe et al. 2010).

10.4.5 Trajectory Simulations in the OAAS Model

The estimates for the spreading of real drifters in the Gulf of Finland (Soomere et al. 2011e, see also Chap. 8) show that it takes, on average, about 4 days for two initially closely located particles to drift into different grid cells of the 2 nm RCO model. This suggests that ignoring sub-grid scale processes may modify a part of the trajectories but their majority will remain at a distance of less than one grid step from their actual position. It is natural to assume that further spreading of the trajectories will mostly occur due to the gradients in the simulated velocity fields. It is also reasonable to suppose that for the particular horizontal resolution and length of trajectories, ignoring the subgrid spreading does not significantly affect the resulting 2D fields and might even suppress the noise in these fields compared to artificial reproduction of the spreading. Doing so is, however, a major simplification that might not be entirely justified (Andrejev et al. 2011).

The trajectories were simulated 'on-line' (simultaneously with the integration of the model, see Chap. 7) in runs of the OAAS model (Andrejev et al. 2010, 2011; Soomere et al. 2011a, 2011b). The scheme accounted for the effect of subgrid-scale motions. Note again that the exact motions of the particles cannot be restored and the major benefit from such efforts is that the statistics of spreading (e.g., the absolute dispersion or the net distance covered by a particle over some time) is represented more adequately.

The impact of subgrid turbulence is usually parameterized by adding certain artificial perturbations to the velocity components of each particle (see Chaps. 4 and 7 for more discussion). The displacement of the particles may be calculated, for example, using the following equations:

$$\frac{d\tilde{x}}{dt} = u_c(\tilde{x}, \tilde{y}) + u', \qquad \frac{d\tilde{y}}{dt} = v_c(\tilde{x}, \tilde{y}) + v', \tag{10.1}$$

where $(\tilde{x}, \tilde{y})$ is the instantaneous location of the particle, (u_c, v_c) are the numerically simulated velocity components from the circulation model and (u', v') are the artificial local velocity perturbations (Andrejev et al. 2010).

The trajectory module of the OAAS model reflects a specific feature of currents in the Gulf of Finland. Jet-like patterns occur seldom here and synoptic eddies cover a large part of the gulf (Andrejev et al. 2004a; Zhurbas et al. 2008). Consequently,

a substantial part of the motions with periods from 2 to 36 h are strongly circularly polarized (Lilover et al. 2011). This feature was accounted for by perturbing the x-component of velocity based on the magnitude of the y-component and *vice versa* (Andrejev et al. 2010). They chose $u' = cr\,v$, $v' = cr\,u$, where the random variable r was uniformly distributed within the interval $[-0.5, 0.5]$ and c was a tunable coefficient reflecting the intensity of spreading.

Setting $c = 0.5$ in Andrejev et al. (2010) resulted in the average spreading rate of 10-day long trajectories in December 1990–November 1991 of about 176 m/day ($\sim$2 mm/s) for the 1 nm model and 10 particles per each grid cell (with a typical initial distance of $\sim$500 m between particles). This value matches the estimates from drift of surface buoys in 2011 for the separation rate of particles initially located at a distance of 50–150 m from each other (Soomere et al. 2011e). The resulting statistics apparently somewhat underestimates the actual spreading rate. The introduced spreading was, though, reasonable to ensure a high enough rate of hits to the nearshore (that was defined as the pool of wet points directly adjacent to the land points): about $2/3$ of all released particles entered this zone during 10 days of propagation (Andrejev et al. 2011).

Each method has its advantages and disadvantages (Chap. 7). The on-line method allows the use of the integration time step of the circulation model for solving the trajectory equations and leads to more exact formal reproduction of single trajectories. This is, however, no real advantage as subgrid-scale effects deform the real trajectories in a manner that can be only reproduced statistically. The set of on-line simulations is severely limited as re-running of a high-resolution circulation model is usually very time-consuming. The accuracy of the trajectories from the off-line method suffers from the coarse temporal resolution of the saved velocity data (usually once in a few hours). This shortcoming is partially balanced by a much larger flexibility: off-line trajectory calculations are much faster, it is easy to re-parameterize the impact of subgrid motions, the already calculated trajectories can be used for differently set problems, etc.

10.5 Quantification of the Risk of Coastal Pollution

The applications described in this book have assumed that a hit of any part of long sections of the nearshore is equally undesired. This is equivalent to introducing a constant cost function: reaching any section of the nearshore by a particle is 'bad' (optionally with a sign) and staying in the open sea (or leaving the test area towards the North Sea or the Baltic Proper) is mostly considered 'neutral.'

10.5.1 Launching the Particles

The basic requirements concerning the number of trajectories in order to create reliable statistics of coastal hits have been discussed in Chap. 9 and in Viikmäe et al.

Fig. 10.2 Major fairways crossing the Gulf of Finland. High-resolution simulation using the OAAS model was performed to the east of longitude 23°27′ E. The *blue line* shows the grid points of the RCO model used for this gulf. Graphics by M. Viška

(2010), Lu et al. (2012). The substantial seasonal variation in the circulation patterns in the test areas requires performing the simulations over at least a few years (Andrejev et al. 2011). In existing applications the simulations have been performed for a five-year test period (May 1987–December 1991 for the Gulf of Finland and 1990–1995 for the SW Baltic Sea). Its length matches the renewal time of Gulf of Finland waters (Andrejev et al. 2004b) and allows for separate consideration of the inflow and outflow patterns in the SW Baltic Sea.

The simulations of trajectories over the entire period in question (typically 5 years in the existing applications) were divided into sequential (optionally partially overlapping) time windows (see Chap. 9). Their length t_w was 10–20 days for the Gulf of Finland and up to 60 days in the Baltic Proper (Viikmäe et al. 2011). At the beginning of each time window, a few (1–10) water particles were selected, usually in all wet points of the circulation model, and their motion was tracked over the time window. In on-line runs the statistics for the time window were calculated immediately and in the off-line runs the results were saved for further analysis.

A subsequent simulation for the same configuration of particles was launched with a certain time lag as described in Chap. 9. The process was repeated over the entire time period of interest. The typical number of time windows ranged from 170 (Andrejev et al. 2010, 2011) up to >10,000 in test simulations with a time lag of 6 hours (Viikmäe et al. 2010). The number of grid cells varied from 2270 in the 2 nm version of the OAAS model (or about 3000 in the RCO model) for the Gulf of Finland up to 31,838 in the 0.5 nm OAAS model in the Gulf of Finland (Fig. 10.2) (Andrejev et al. 2010). The number of selected particles was reduced in Lu et al. (2012) by choosing only every fourth cell of the ocean model for seeding of particles. The usual number of trajectories per grid cell was on the order of 1,000–10,000.

10.5.2 Indicators of Coastal Hit and Drift Time

The quantification procedure of the offshore domains used standard statistical analysis of auxiliary variables p_{ij}^{mk} and a_{ij}^{mk} associated with each released particle. Here,

(i, j) indicate the grid cell in Cartesian coordinates, m is the sequential number of particles in this cell and k is the number of time window. For example, setting the variable $p_{ij}^{mk} = 0$ initially and switching it to 1 when the particle hits the nearshore for the first time, is convenient for estimates of the probability of coastal hits (Andrejev et al. 2010, 2011). A zero value of p_{ij}^{mk} at the end of a time window means that the particle has only been offshore or has left the test area through the open boundary.

The time during which the particle has drifted in the basin without touching the coast can be measured by assigning to another variable a_{ij}^{mk} the time elapsed from the beginning of simulations until the particle hits a nearshore for the first time. If the particle does not hit the coast, a_{ij}^{mk} is assigned the length of the time window. The results of this method applied for sea areas with an open boundary may substantially depend on how exactly the particles that drift out of the computational area are handled (Soomere et al. 2011c).

The cell-wise probabilities of coastal hits $P_{i,j}^{(k)}$ and particle age $A_{i,j}^{(k)}$ were calculated for each time window k as the average of the relevant values p_{ij}^{mk}, a_{ij}^{mk} over M particles released into a particular cell (i, j):

$$P_{i,j}^{(k)} = \frac{1}{M}\sum_{m=1}^{M} p_{ij}^{mk}, \qquad A_{i,j}^{(k)} = \frac{1}{M}\sum_{m=1}^{M} a_{ij}^{mk}. \tag{10.2}$$

The cumulative average probability $\bar{P}_{i,j}$ for the coastal hits and the cumulative average age $\bar{A}_{i,j}$ in a particular cell for the first n time windows were defined in the classical manner:

$$\bar{P}_{i,j}(n) = \frac{1}{n}\sum_{k=1}^{n} P_{i,j}^{(k)}, \qquad \bar{A}_{i,j}(n) = \frac{1}{n}\sum_{k=1}^{n} A_{i,j}^{(k)}. \tag{10.3}$$

Setting the parameter n in (10.3) equal to the total number of time windows $N_{\max}$ gives the estimates for the probability of a coastal hit and the particle age at the particular grid cell over the entire simulation period. The resulting values for single cells $p_{ij} = \bar{P}_{i,j}(N_{\max})$ and $a_{ij} = \bar{A}_{i,j}(N_{\max})$ constitute the pixels of the spatial maps reflecting two possible quantifications of the offshore areas. Similarly, one can define the average probability for coastal hits (or particle age) for any sea domain of interest by further averaging over the resulting values p_{ij} or a_{ij} for cells in this area, or, alternatively, for a selected season or other time interval.

The resulting average time for the coastal hit (particle age) is similar to commonly used water age (Deleersnijder et al. 2001) that has been extensively studied for the Baltic Sea (Engqvist et al. 2006) and Gulf of Finland (Andrejev et al. 2004a, 2004b). The difference is that here the time is defined following the Lagrangian framework for limited-duration trajectories ending at the nearshore while the majority of earlier studies use Eulerian velocities and other specifications of the age.

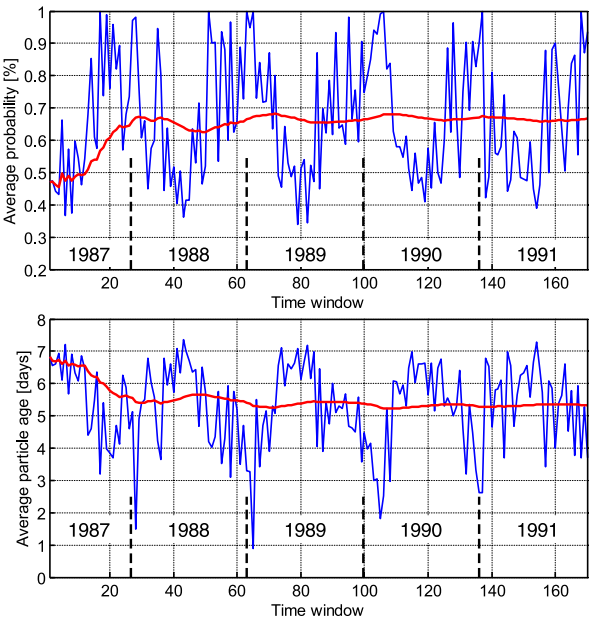

Fig. 10.3 Mean probability $P(k)$ for particular time windows (*blue*) and cumulative average probability $\bar{P}(n)$ (*red*) (*upper panel*); mean particle age $A(k)$ for particular time windows (*blue*) and cumulative average particle age $\bar{A}(n)$ (*red*) (*lower panel*) in the Gulf of Finland based on the 1 nm OAAS model for May 1987–December 1991 (Andrejev et al. 2011)

10.5.3 Long-Term Course of Probability and Particle Age

The temporal behaviour of the average probability $P(k) = \langle P_{i,j}^{(k)} \rangle$ and particle age $A(k) = \langle A_{i,j}^{(k)} \rangle$ over all particles for a particular time window k (Fig. 10.3) allows a rough estimate of the length of the time interval to be covered in order to reach climatologically valid results. The angled brackets denote the arithmetic mean over all sea points in the calculation area. Their behaviour was analysed in Andrejev et al. (2011) using the 1 nm OAAS model and above-discussed on-line trajectory calculation scheme. The modelling period of 1 May 1987–31 December 1991 was divided into 170 consecutive 10-day long time windows. At the beginning of each window ten particles were released into each surface grid cell and locked in the uppermost layer.

The fluctuations in the cumulative values $\bar{P}(n)$ and $\bar{A}(n)$ rapidly decreased when n increased. Their changes only partially followed the patterns in forcing factors. During the first months of calculations (the calm period of May–June 1987) the values of $\bar{P}(n)$ were about 0.48 (Fig. 10.3). Over the subsequent windy season, until February 1988, the kinetic energy density of surface wind increased by a factor of three (Soomere et al. 2011a) but $\bar{P}(n)$ only increased by about 30 % (Fig. 10.3). The seasonal course of the mean particle age $A(k)$ was, as expected, in antiphase with $P(k)$ (Fig. 10.3). The largest probabilities for coastal hits occurred roughly simultaneously with the smallest particle age during autumn and winter storms.

Both the quantities $P(k)$ and $A(k)$ exhibited substantial short-term variations with amplitudes comparable with or even larger than their seasonal variations (Fig. 10.3). In particular, $P(k)$ revealed especially pronounced seasonal variation,

from about 0.4 (mostly in calm seasons) to values very close to 1. Their relative fluctuations were, however, much smaller than similar variations in the forcing factors. For example, monthly averaged kinetic energy density of surface wind varied by more than 10 times in the Gulf of Finland (Andrejev et al. 2011).

Both the cumulative quantities already closely matched their asymptotic values $\bar{P}(N_{\max}) \approx 0.67$, $\bar{A}(N_{\max}) \approx 5.3$ days after the first half-year of simulations and revealed moderate variations after about two years of calculations. Their short-term and seasonal fluctuations were very small (about 3 % from the average) from the third year on and were almost negligible (below 1 %) after the fifth year. Therefore, the cumulative measures in question calculated over >3 years reflect well long-term internal properties of current-driven transport patterns even in a domain hosting extensive seasonal variations in the forcing pattern such as the Gulf of Finland. This time scale is close to the average 'classical' water age (equivalently, the time scale of renewal of water masses) in the Gulf of Finland (Andrejev et al. 2004a) that also revealed very small changes after three years of simulations.

The asymptotic values $\bar{P}(N_{\max})$ and $\bar{A}(N_{\max})$ can be used to roughly evaluate whether the parameters of the developed procedure are sensible. The overall probability of coastal hits had a reasonable level $\bar{P}(N_{\max}) \approx 0.67$, not very close to 1 and also not small. It signifies that about 2/3 of the released particles have contributed to the estimates of the environmental risk. The limit value of the particle age was somewhat smaller than might be expected based on Viikmäe et al. (2010) where typically only 30–40 % of the particles released in the central part of the gulf reached the nearshore within 10 days. Finally, we note that both $P(N_{\max})$ and $A(N_{\max})$ may depend on the length of the time window t_w in use. This dependence is usually much stronger for $A(N_{\max})$, as t_w is assumed to be the age of all particles that have not reached the coast (Soomere et al. 2011c, 2011d).

10.5.4 Spatial Distributions of Probability and Particle Age

The most important intermediate products of the technology are spatial distributions of the measures of the environmental risk $p_{ij}(x, y)$ and $a_{ij}(x, y)$ associated with the release of pollution. These maps can serve as starting points of various engineering applications and decision support systems.

The average probability of a coastal hit for single cells p_{ij} over the entire simulation period shows a rich spatial structure for the test areas (Fig. 10.4). The probabilities to the west of Paldiski (Fig. 10.2) in the Gulf of Finland are strongly affected by the presence of the open boundary. The areas with smallest $p_{ij} < 0.4$ are located far offshore. The regions of small p_{ij} have relatively small gradients. This is partially caused by the choice of the length of the time window (10 days) an increase in which eventually would lead to larger contrasts in p_{ij} (Soomere et al. 2011c).

A wide area where $p_{ij} \sim 0.5$–0.6 extends from Lahemaa almost to the island of Gogland. Its bend to the south into Narva Bay obviously reflects the presence of islands (that are ignored in the 2 nm simulations of Soomere et al. 2011c). Smaller

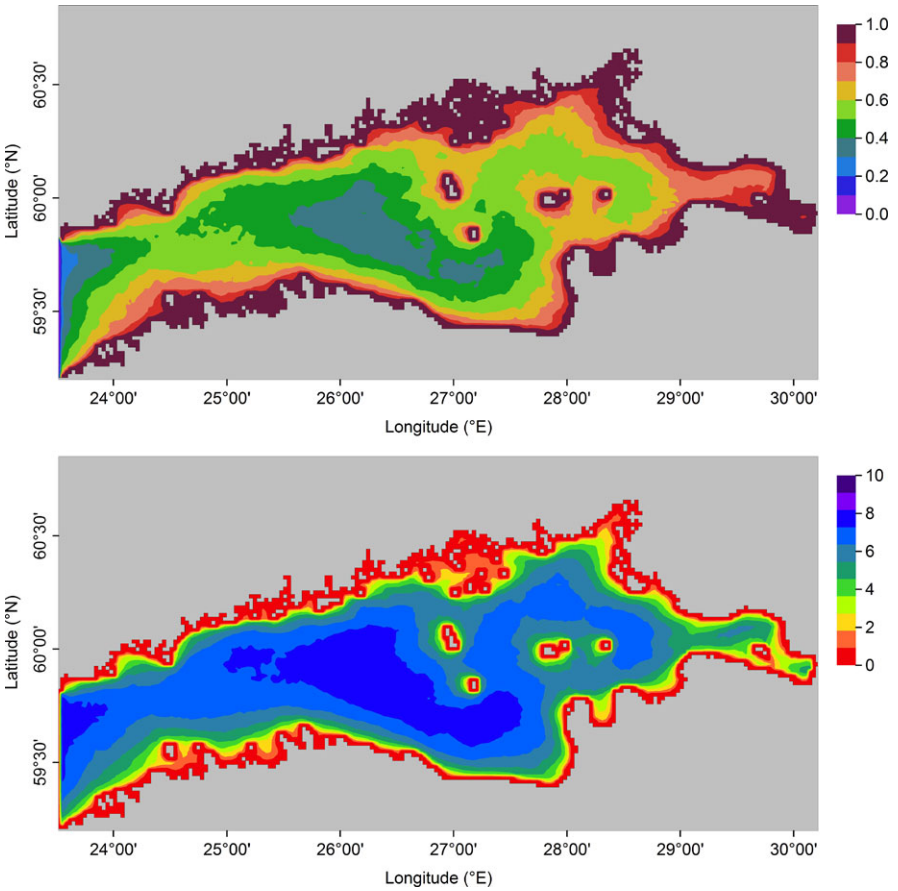

Fig. 10.4 Probabilities of hitting the coast (*above*) and particle age (days, *below*) for May 1987–December 1991 calculated using the 1 nm OAAS model and 10-day long trajectories (Soomere et al. 2011c)

areas of this probability level are in the easternmost part of the gulf and between Tallinn and Helsinki.

The particles released at a distance <3–4 km from the coast almost surely ($p_{ij} > 0.9$) hit the coast within 10 days. The probability for coastal hit is high ($p_{ij} > 0.8$) in the entire Neva Bay. A relatively wide belt of high p_{ij} characterizes the coastline sections with complex geometry such as Lahemaa or the vicinity of Tallinn Bay. Its dimensions might be interpreted as the width of the coastal zone. This zone is frequently specified based on a high residence time of water near the coast (see, for example, Lessin et al. 2009). A large probability p_{ij} in the nearshore areas obviously signifies low persistency of water masses, while a small p_{ij} may simply mean that the net transport is directed to the offshore (Soomere et al. 2011a). A wide coastal zone exists in this sense along the Finnish coast, NE coast of the gulf

and from Lahemaa to Paldiski along the southern coast of the gulf. On the contrary, an intense exchange of water with the offshore is typical for Narva Bay and NE coast of Estonia.

The areas with relatively large particle age are located, as expected, far from the coasts and islands. Their spatial distribution (Fig. 10.4) mirrors the properties of a similar distribution for the probabilities such as a rich internal structure and a certain asymmetry in the North-South direction. The distribution of the particle age in areas with $a_{ij} > 6$ days is obviously smoothed to some extent owing to the use of 10-day long time windows. The largest values of particle age and the smallest probabilities are located in areas considerably shifted to the north from the geometrical axis of the gulf in the narrowest part of the gulf between Tallinn and Helsinki. These areas do not necessarily coincide with domains that have the longest distance to the coast. This implicitly reflects the anisotropy of the surface currents and signifies that the entire approach leads to nontrivial results for the Gulf of Finland.

10.5.5 Dependence on Spatial Resolution

The discussed properties obviously depend on the ability of the circulation model to represent the geometry and bathymetry of the basin and to resolve mesoscale motions. The dependence of the distributions of probabilities and of the particle age on the model resolution was studied using the OAAS model with spatial resolutions of 2, 1 and 0.5 nm and otherwise identical setup, forcing and boundary conditions. The number of sea points in the calculation area was 2270 for the 2 nm model, 8810 for the 1 nm model and 31,838 for the 0.5 nm model (Andrejev et al. 2010).

The temporal behaviour of the mean probability $P(k)$ and particle age $A(k)$ for particular time windows, and their cumulative values $\bar{P}(n)$ and $\bar{A}(n)$ was very similar for all horizontal resolutions (Fig. 10.5). The time series of $P(k)$ and $A(k)$ are highly correlated (for example, $r = 0.98$ for the 1 nm and 0.5 nm simulations) and have small bias, mean and root-mean-square deviation, and also a very low level of spread. The standard deviations for the pointwise values from the average values of $P(k)$ and $A(k)$ are almost the same for different resolutions (Andrejev et al. 2011). This suggests that the variations in these fields with respect to the mean values have, on average, a similar structure.

The estimates of the asymptotic values $\bar{P}(N_{\max})$ and $\bar{A}(N_{\max})$ are practically insensitive to the resolution of the ocean model. Therefore, these quantities are to some extent similar to certain scalar fields such as salinity and temperature that are also well represented by eddy-permitting models starting from a 1 nm resolution.

The resolution of the ocean model affects to some extent the 2D maps of the probability p_{ij} and particle age a_{ij} (Fig. 10.6). The overall appearance of these maps, the location of the isolines and the areas of low probabilities and high particle age largely coincide for all resolutions. The largest differences between the relevant maps at the resolutions of 1 nm and 0.5 nm are in the size of the areas of the smallest

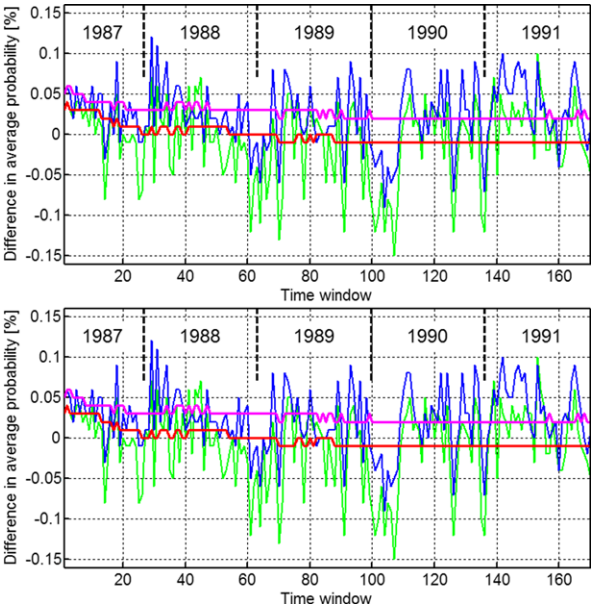

Fig. 10.5 Difference between the mean probability $P(k)$ and the cumulative average probability $\bar{P}(n)$ (*upper panel*) and the mean particle age $A(k)$ and its cumulative value $\bar{A}(n)$ (*lower panel*) calculated at different horizontal resolutions of the OAAS model. *Green* and *red*: difference between the results of the 1 nm and 2 nm models; *blue* and *magenta*: difference between the results of the 1 nm and 0.5 nm models (Andrejev et al. 2011). The results for the 1 nm model are shown in Fig. 10.4

probabilities ($p_{ij} < 0.4$) and the areas of the largest particle age ($a_{ij} > 8$ days): domains of very small probability or of large particle age are larger in the calculations with the 1 nm model.

The accuracy of the representation of islands and bathymetry obviously is most important with respect to these differences. Only the few largest islands are represented in the 2 nm OAAS model. An increase in the resolution evidently leads to a much better reproduction of mesoscale eddies and smaller-scale flow features The presence of the Finnish archipelago and many small islands, such as Keri to the north of Prangli, Sommers (Someri) between Gogland and Vyborg, and Malyj Tjuters (Pieni Tytärsaari, also Väike Tütarsaar) to the NE of Kunda at the 0.5 nm resolution (Fig. 10.2) obviously leads to a reshaping of the areas with high p_{ij} and low particle age.

The presence of islands and the more exact representation of the bathymetry of the Gulf of Finland (Andrejev et al. 2010) are evidently responsible for a relatively high level of local fluctuations in the fields of p_{ij} and a_{ij} at the 0.5 nm resolution. Although a significant increase in the complexity of the fine structure of the resulting fields is evident in Fig. 10.7 for the 0.5 nm model, the shape and location of the isolines are almost the same. The increase in resolution is accompanied by an increase from 4 to 16 times in the number of evaluated trajectories, which definitely improves the accuracy of the estimates for sea domains of fixed size.

The areas of minimal probability (maximal age) correspond well with sea areas hosting either relatively intense westward subsurface transport or with domains with quasi-steady eddies (cf. Fig. 11 of Andrejev et al. 2004a). This match suggests that these eddies reflect the gulf's bathymetry rather than dynamic mesoscale features. Such a 'geometric' determination of the location of eddies evidently enhances the

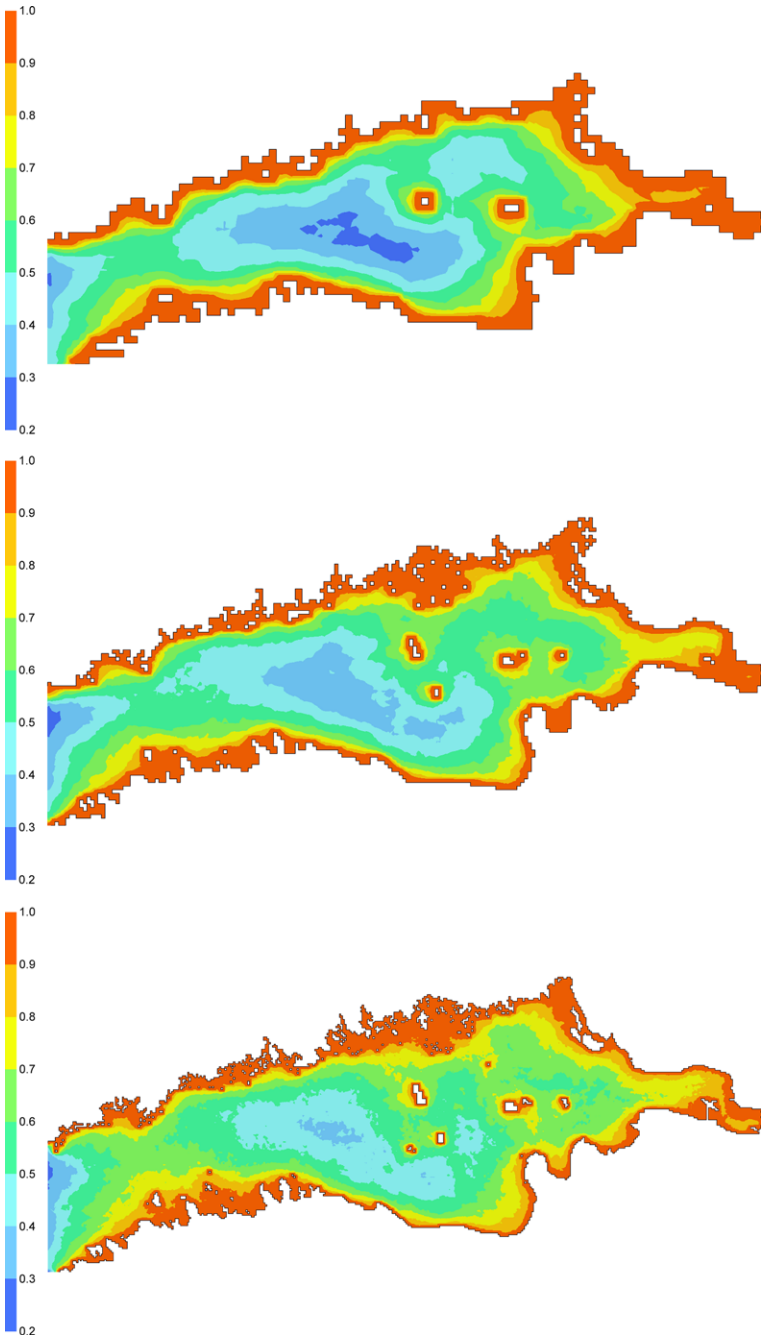

Fig. 10.6 Probability of a coastal hit in the Gulf of Finland simulated with the use of the OAAS model with a resolution of 2 nm (*upper panel*), 1 nm (*middle panel*) and 0.5 nm models (*lower panel*) for the period 1987–1991 (Andrejev et al. 2011)

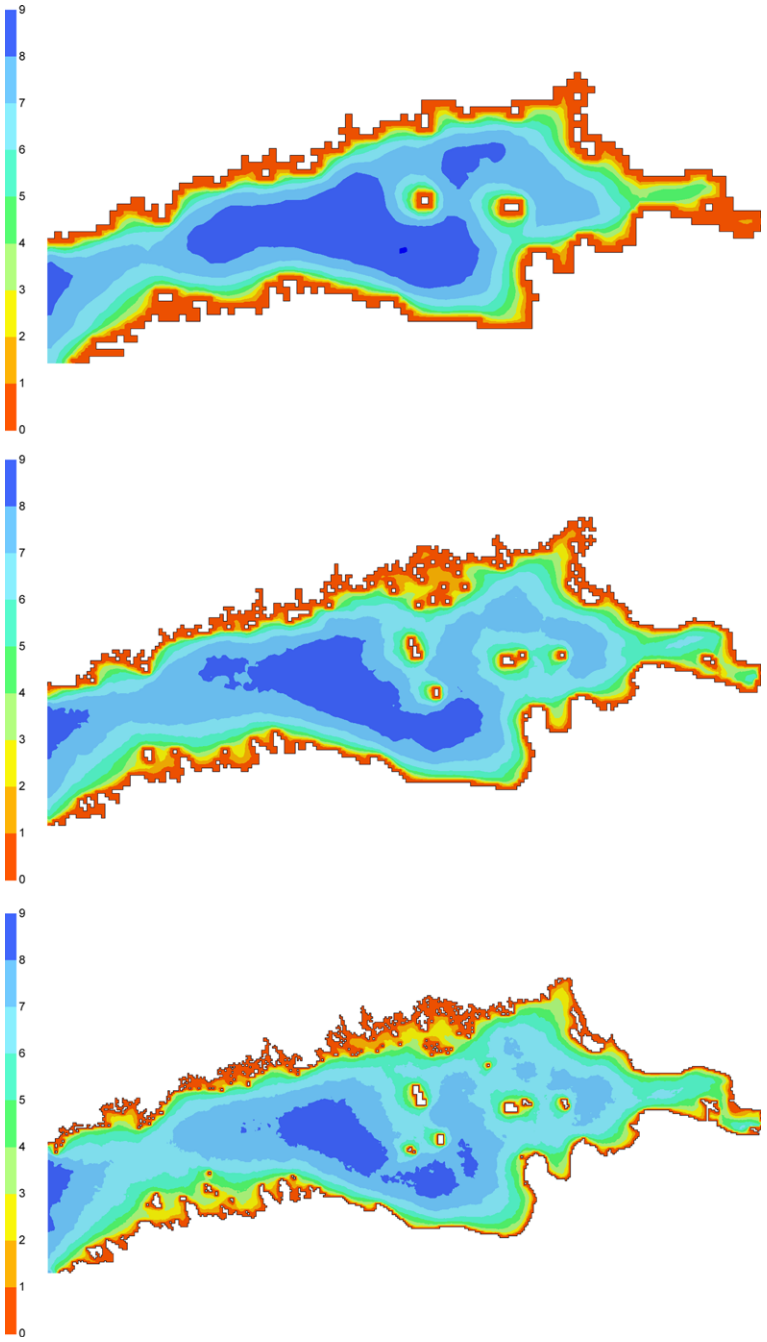

Fig. 10.7 Particle age in the Gulf of Finland simulated with the use of the OAAS model with a resolution of 2 nm (*upper panel*), 1 nm (*middle panel*) and 0.5 nm (*lower panel*) for the period 1987–1991 (Andrejev et al. 2011)

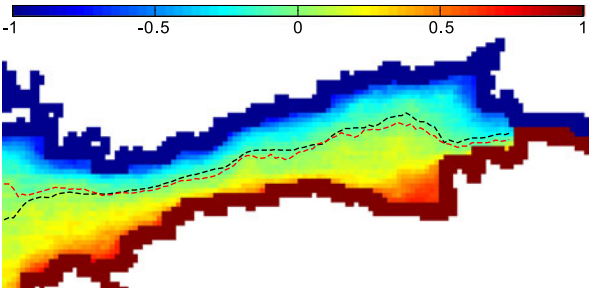

Fig. 10.8 Distribution of $\hat{p}$ characterizing the probability of hitting the northern and southern coasts using the smoothing method and $t_w = 20$ days. *Black* and *red lines* indicate the equiprobability lines for the direct and smoothing methods, respectively (Soomere et al. 2011c)

similarity of the results obtained with the models at 1 nm and 0.5 nm resolution as both these models reasonably reproduce the bottom shape.

10.6 Applications for Decision-Making

10.6.1 Sharing the Costs: the Equiprobability Line

Many elongated sea areas are divided between different countries. In such cases it is of interest to specify the (equiprobability) line so that the probability of transport of the pollution released at this line to the opposite coasts would be equal. This situation has clear practical importance for the Gulf of Finland: Estonia is located on the southern coast and Finland on the northern coast so that the dividing line largely follows the centreline of the water body. An appropriate quantification of the offshore domains in this framework is possible by assuming the 'costs' of hitting the opposite coasts equal in the magnitude of 'badness' but having opposite signs.

This approach was employed in Soomere et al. (2010, 2011c) using the 2 nm RCO model data for 1987–1991, the TRACMASS code, 10 or 20 day long trajectories, the time lag between realizations of 1 day and the specification of the nearshore as a 3 grid cell (about 11 km) wide belt (Viikmäe et al. 2010). Differently from the above calculations with the OAAS model, the presence of islands was entirely ignored.

The problem was addressed using two methods that only differed from each other by the number and the location of the particles. The *direct method* (called Method I below) tracked four particles released in each grid cell. A counter for a cell was initially set to 0 and switched to ± 1, when at least three out of these reached one and the same nearshore (-1 for the northern and $+1$ for the southern coast). The averaging procedure was exactly the same as described above. The resulting quantity $\hat{p}$ was in the range of $-1 \le \hat{p} \le 1$ (Fig. 10.8) where $\hat{p} \approx 1$ and $\hat{p} \approx -1$ stood for a high probability of hitting the southern and the northern coast, respectively.

Another (*smoothing*) *method* (Method II) accounted for the drift of particles in a cluster of nine cells. The counter was set to ± 1 when ≥ 5 particles released into the centres of the cell of interest and into the eight cells surrounding it reached one and

the same coast. In early simulations using 10-day long trajectories (Soomere et al. 2010) the separation point of the opposite coasts was set at the mainland border between Estonia and Russia at the River Narva mouth in the SE of the Gulf of Finland (28°2′ E, 59°27.5′ N). In later simulations with the same model and 20 day long trajectories, the separation point was set at the mouth of the River Neva (Soomere et al. 2011c).

The equiprobability line followed the gulf axis in the narrowest part of this water body, deviated substantially to the north of it at the gulf entrance and in the widest part of the gulf, and came quite close to the southern coast of the easternmost narrow part of the gulf. While the latter feature evidently mirrors the flow of the voluminous runoff from River Neva that merges with the overall cyclonic circulation in the gulf in this area (Chap. 6), the two other deviations of the equiprobability line from the centreline of the gulf apparently signify certain systematic anisotropic features of the transport by surface currents.

10.6.2 Cross-Sections

Different cross-sections of the distributions of the probability, the particle age and the quantity $\hat{p}$ characterizing the probability of hitting the opposite coasts of the Gulf of Finland reveal several important features of the underlying fields (Fig. 10.9). For relatively narrow parts of the gulf all the fields have a clearly defined extremum or zero-crossing. A deviation from these points by only a few km is associated with a considerable change in the values of the underlying quantities (equivalently, in the environmental risks). Interestingly, the exact locations for the optimum values (potential locations for the sailing line) not necessarily coincide for different measures even in the narrowest part of the gulf.

While the zero-crossings of $\hat{p}$ are usually located very close to the gulf axis, the extrema of other fields may be substantially shifted to either side. The largest deviations are shown by the locations for the longest particle age for a particular longitude. The particularly large deviation of these locations for the two ways of interpreting the fate of particles that drift out of the gulf demonstrates the sensibility of the entire approach on the underlying value system.

Another significant feature of the cross-sections of relatively wide sections of the gulf is the presence of a wide area of low cross-gulf gradients in which the values of the underlying distributions reveal quite limited changes. This area can be naturally identified as an area of reduced risk. In most occasions this area ends abruptly, and relocation of a potentially dangerous activity closer to the coast is associated with a rapid increase in the relevant risks. The presence of a well-defined bend in the cross-sections in Fig. 10.9 indicates a possibility for systematically selecting a reasonable distance from the coast for possible sources of environmental risks. This feature can be particularly useful for the specification of the minimum acceptable distance from the coast for tanker routes along open ocean coasts.

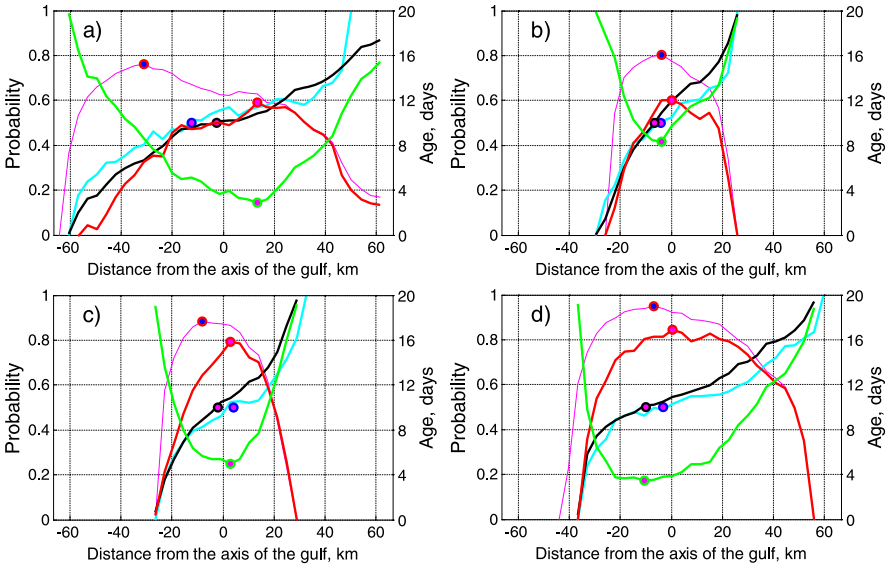

Fig. 10.9 Examples of cross-sections of probabilities for coastal hits (*green*), particle age (Method IVa: *red*, Method IVb: *magenta*; see below Sect. 10.7.3 for the explanations) and for the quantity characterizing the probability of hitting the northern and southern coasts (direct method: *black*; smoothing method: *cyan*, both shown as $(\hat{p}+1)/2$: for the gulf entrance (**a**), western narrow part (**b**), middle of the gulf (**c**) and for the wider part of the gulf between Narva and Kotka (**d**). *Circles* indicate the optimum location of the potentially dangerous activities (Soomere et al. 2011c). The location of cross-sections is shown in Fig. 10.10

10.6.3 Simplest Optimum Fairways

The calculated distributions can be used as a support for decision-making in a variety of problems. The global minimum of the probability of coastal hits and similarly the maximum of the particle age indicate a climatologically valid approximate solution for a stationary location of a potentially dangerous activity, for example, a drilling rig, an oil platform, or a crossing point of ship traffic.

An important application is the environmental management of ship traffic in terms of minimizing the consequences of potential release of contaminants. Examples of the quantity $\hat{p}$, the probabilities of coastal hit and the particle age have been used in different applications. Regardless of which particular measure for the quantification of the offshore has been used, the goal was to determine the location of the optimum fairway (more generally, the pathway for a moving source of pollution) based on the obtained distributions.

The technique will be discussed here using an example of environmental risks associated with current-driven coastal pollution but it is obviously applicable to construct an optimum for virtually any set of cost distributions of possible accidents generated by the definition of valuable or vulnerable areas in terms of any convenient measure of the environmental or economic risk. We start from an idealized

case when the length of the optimum fairway does not play a role and the basic goal is to minimize the average probability of coastal hit or to maximize the particle age along the fairway or to share costs equally.

If the intention is to divide costs equally, an inherent approximation to the optimum solution is the equiprobability line (Soomere et al. 2010). Sailing along this line naturally results in dividing the potential costs equally between the opposite coasts: a deviation from it to either side increases the projected costs of consequences for this side. It is heuristically clear that the equiprobability line generally does not provide a global minimum for environmental risks. This solution is only suitable for elongated basins and accounting for the presence of islands may be complicated.

For a sea area of elongated shape the maps of probability of coastal pollution and of particle age, ideally, provide an elongated 'trough' of low values for probabilities or, equivalently, a similar 'crest' of particle age, and a more or less gently sloping pattern of the measure $-1 \le \hat{p} \le 1$ between the opposite coasts. Figures 10.7–10.9 suggest that the resulting fields generally have one local extremum of the probability and age (and also one zero-crossing point of the quantity $\hat{p}$) for all cross-sections of the Gulf of Finland except for the entrance and for the easternmost part of the gulf. It is natural to assume that the optimum fairway goes roughly along this trough or crest, or follows the zero-crossing line of $\hat{p}$.

In practical applications the underlying data for Figs. 10.7–10.8 were first corrected manually in order to adjust a few clearly erroneous values (zeros of the probability or very large values of the particle age) for several bays deeply cut into mainland. In the model resolution, currents in these areas were very small and almost no particle propagation occurred in the RCO model that worked without local spreading. The latitude for the points of the optimum fairway was found from the analysis of the cross-section of the relevant field along each longitude (Fig. 10.9). It was set at the centre of the grid cell corresponding to either the minimum probability p_{ij} or the maximum particle age p_{ij} (Soomere et al. 2011c; Lu et al. 2012). The obtained estimates for the optimum fairway were confined to discrete values of the centres of grid cells and sometimes contained abrupt shifts by 2–3 cells to the south or north. Optionally the curves were smoothed over five neighbouring values in the east–west direction (Fig. 10.10).

Another estimate of the optimum fairway roughly following the equiprobability line was constructed from the zero-crossing points of the measure $\hat{p}$ (Soomere et al. 2010). These points were well defined in the relatively narrow parts of the gulf that hosted comparatively large north–south gradients of $\hat{p}$. The small-scale fluctuations in the distribution of $\hat{p}$ in some parts of the bay (especially in the eastern part where its north–south slope was small) were smoothed by averaging the cross-section over five neighbouring grid points. An estimate for the zero-crossing of $\hat{p}$ for each longitude was found using a linear approximation between its smoothed values at adjacent grid points. Doing so led to a single clearly defined zero-crossing point for each longitude. The curves consisting of the zero-crossing points required no additional smoothing in the east–west direction (Soomere et al. 2011c).

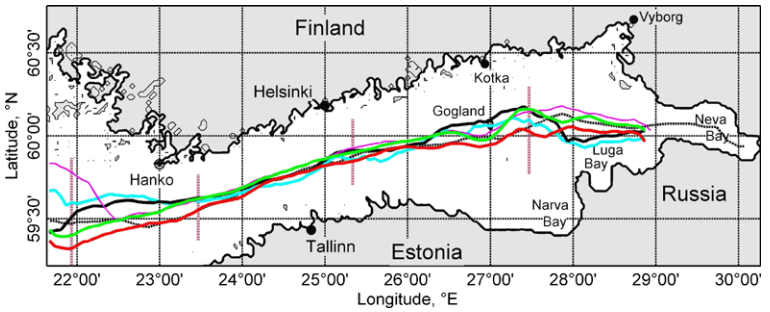

Fig. 10.10 The location of the optimum fairways based on Methods I–IV (see Sect. 10.7.3). The *colour code* is the same as for Fig. 10.9. The *dotted black line* indicates the geometrical centreline of the gulf for the 2 nm grid and the *vertical lines* correspond to the cross-sections in Fig. 10.9. Note that the location of smoothed optimum fairways may slightly deviate from those indicated in Fig. 10.9 (Soomere et al. 2011c)

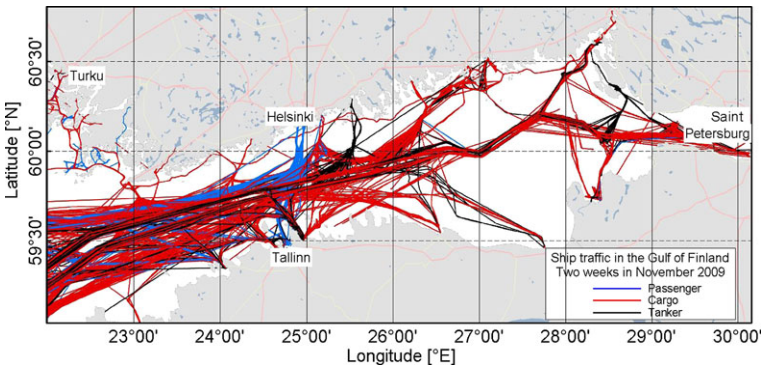

Fig. 10.11 Trajectories of ships in the Gulf of Finland over two weeks in November 2009 (Soomere et al. 2010). Data courtesy HELCOM

10.6.4 Following Local Decisions

For regions with complicated geometry and strongly heterogeneous transport patterns the shape of the relevant distributions may be quite complicated; for example, certain cross-sections may host several extrema. A simple algorithm to obtain a first approximation for the optimum fairway was introduced in Andrejev et al. (2011). It accounts for a specific pattern of the ship traffic in the Gulf of Finland (Figs. 10.2, 10.11) and is based on local properties of the underlying measures. The majority of cargo ships (including tankers that carry the largest potential for pollution) sail from the Baltic Proper to large harbours in the eastern part of the gulf (HELCOM 2009).

The easternmost point of the fairway for ships sailing to the Saint Petersburg area was chosen near the destination harbour. The next point was selected as the one corresponding to the minimal probability of a coastal hit (or the maximal particle age,

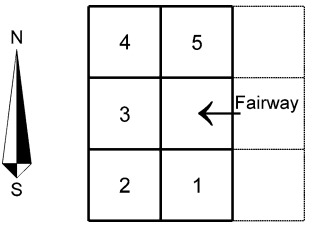

Fig. 10.12 The simple algorithm for calculating an optimum fairway. The next fairway point is chosen from among the centres of cells 1–5 or 2–4 adjacent to the instantaneous location of the ship (marked by the *arrow*)

or the smallest $|\hat{p}|$ among the five adjacent grid points in the main sailing direction (Fig. 10.12). The process was repeated until the fairway reached the Baltic Proper. The resulting fairway may head to the north or south for some periods of time but cannot go back.

Fairways constructed using this algorithm and based on the probability for the coastal hits (Fig. 10.13) follow the identical route along most of the Gulf of Finland and diverge to the different destinations about half-way from the Helsinki–Tallinn line to Gogland. The fairway to Vyborg is located asymmetrically, mostly to the north of the centreline of the gulf, suggesting that a southward surface drift prevails almost everywhere except possibly to the north of Lahemaa. This feature suggests that the anticyclonic gyre identified for the surface layer of the Gulf of Finland in the 2 nm RCO simulations (Soomere et al. 2010) is implicitly evident also in the simulations with a higher resolution.

As the general appearance of the distributions for the probabilities (Fig. 10.4) and the particle age (Fig. 10.7) is fairly similar, it is not unexpected that the corresponding optimum fairways quite closely follow each other (Fig. 10.13). They are mostly located to the north of the gulf axis (by 2–8 km on average) and meander substantially in some sections. They almost overlap in the relatively narrow part of the gulf between Naissaar and Porkkala and in narrow passages between islands, e.g., to the south of Gogland (Fig. 10.2). They deviate up to 20 km from each other in the widest sections of the gulf where the gradients of the underlying fields are small (cf. Fig. 10.9).

Surprisingly, the two optimum lines also considerably deviate from the axis of the gulf in the very narrow area between Tallinn and Helsinki that hosts extremely heavy crossing cargo and passenger traffic (HELCOM 2009). If the fairways were allowed to exert local turns by up to 135°, they may follow a northern route between Gogland and the Finnish archipelago. Such a large difference between the results of quite similar methods of fairway construction highlights the influence of the local decision at each grid cell on the overall shape and parameters of the optimum sailing line and certainly calls for the implementation of more elaborated approaches to specify a globally optimized fairway.

In essence, the described procedure is a discrete variant of the method of the least steep gradient for finding crests or troughs on a 2D map of elevations in which all the decisions are made locally. If the underlying measure (p_{ij}, a_{ij} or $\hat{p}_{ij}$) has exactly one minimum, maximum or zero-crossing across the gulf, the process obviously finds and follows it. The template for the next point in Fig. 10.12 can be rotated in order to fit with the general direction of the fairway, which for example goes to the

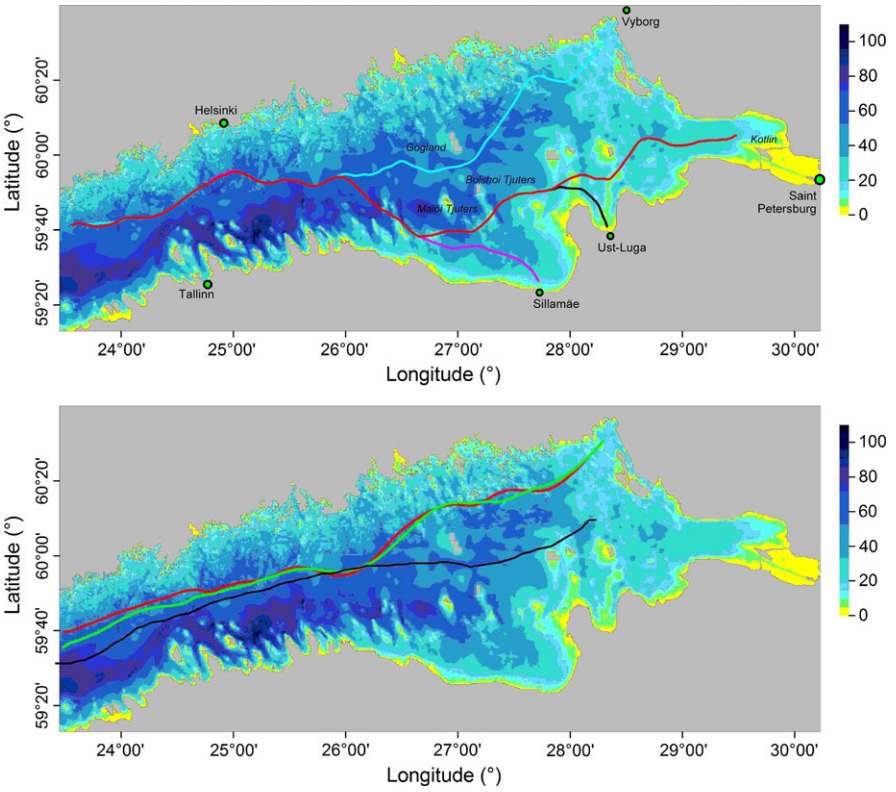

Fig. 10.13 *Upper panel*: Optimum fairways to Vyborg, Saint Petersburg, Ust-Luga and Sillamäe based on the probabilities for the coastal hits calculated for 1987–1991 using the 1 nm OAAS model (Fig. 10.6) and an additional restriction that the local turn of the fairway should not exceed 90° at each point (Andrejev et al. 2011). The fairways are smoothed over 7 subsequent points. The underlying bathymetry (depth in metres) is from Andrejev et al. (2010). *Lower panel*: optimum fairways from Vyborg to the Baltic Proper based on spatial distributions of probabilities for the coastal hits (*blue*) and particle age (*red*) with no restrictions to the local turn of the fairway. The *black line* indicates the centreline of the gulf (Soomere et al. 2011b)

north after passing through the Great Belt (Fig. 10.14). The obvious shortcoming is that the rotation of the template to force the optimum fairway to head to the desired destination can only be made in 45° steps.

The process frequently leads to extensive excursions of the resulting path across the main sailing direction (Fig. 10.14). The resulting fluctuations may be suppressed, for example, iteratively after the entire fairway has been specified (Soomere et al. 2011b). Another way of receiving more smooth optimum sailing lines *ab initio* is to restrict the local turns in the sailing direction. A simple way of doing so is to search the next point among three adjacent cells located strictly in the main sailing direction (cells 2–4 in Fig. 10.12) (Andrejev et al. 2011).

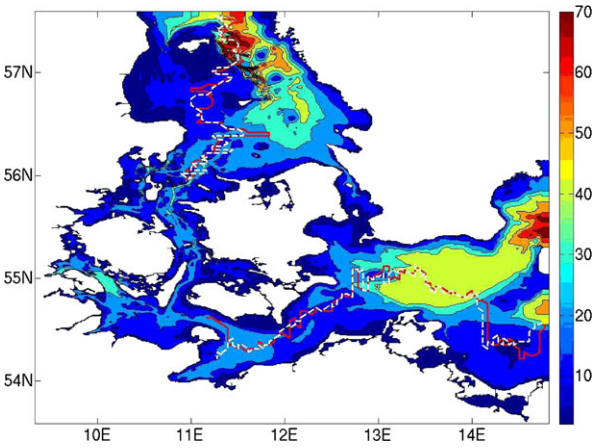

Fig. 10.14 A selection of optimum fairways in the SW Baltic Sea based on the probability for coastal hits (*red*) and particle age (*white*) for the period of 1990–1994 on the background of bathymetry (depth in metres) (Lu et al. 2012, modelling and visualization by X. Lu and E.V. Stanev)

A less obvious feature is that the process is not symmetric with respect to the change in the search direction. In the case of the Gulf of Finland it generally fails to establish the optimum fairway for ships sailing eastwards because the optimum line not necessarily approaches the destination harbour. In general, the systematic use of spatio-temporal variations in these distributions in order to minimize environmental risks is a complicated 2D optimization problem.

There exist much more elaborated methods for finding an optimum line over a 2D field such as Dijkstra's algorithm (used in Höglund and Meier 2012 for solving a similar problem based on Eulerian transport), discrete versions of the variational method, or methods based on Monte Carlo simulations (see Chap. 11 for a description of some alternatives). The main purpose of the presented exercises is, however, to demonstrate that even the use of a very rough estimate for the optimum fairway has a clear potential for a substantial benefit in certain environmental terms, expressed either as a considerably smaller probability for a coastal hit or as a clearly larger time for reaching the coast.

10.7 The Benefit and Uncertainties

One consequence from the vast variety of ecological values and indicators of environmental well-being (Rice 2003) is that the estimates of the benefit enormously depend on the particular choice of the value system. In this context an instructive feature of the presented exercise is not only the invariance of some estimates of the gain from options in calculations but, more importantly, the potential increase in the basic quantitative measures of environmental risks.

10.7.1 Quantification of the Benefit

The simplest estimates of the benefit for a stationary location of a potentially dangerous activity that has to be carried out in the open sea are the ratio of the minimum probability $\min(p_{ij})$ and the average probability $\bar{P}(N_{\max})$, and the difference between the maximum $\max(a_{ij})$ and average particle age $\bar{A}(N_{\max})$. The typical values of $\bar{P}(N_{\max})$ are in the range from 0.62 to 0.67 in the Gulf of Finland (Andrejev et al. 2011; Soomere et al. 2011c) whereas the minima of the probability extend well below 0.3. In realistic conditions there exist many constraints for the location of such spots and the benefit has to be estimated by comparing the extrema of the particular measure with its average values over the technically suitable sea domain.

For certain choices of measures only the additional 'costs' of the consequences can be estimated. An example is that the equiprobability line only divides equally the potential loss between the opposite coasts. The relevant measure $\hat{p}_{ij}$ contains very limited information about the actual probability of the coastal hit. The benefit from its use can be measured to some extent as the average value of $\hat{p}$ (either for a particular location or for a fairway roughly following this line) showing the added risk for one side.

Similarly the potential benefit from the use of an optimum sailing line substantially depends on the underlying measure, the value system and additional constraints. The simplest way to estimate the benefit from the use of the sailing line that provides a reduced level of probability of coastal hits in case of possible accidents can be roughly evaluated in terms of the decrease in the probability of such a hit compared with a 'random' location of the fairway. A convenient measure is the ratio $p_{\mathrm{opt}}/\bar{P}(N_{\max})$ of this probability p_{opt} calculated along the optimum fairway over the average probability for the entire sea. In these terms the benefit is quite substantial. For example, for the 2 nm RCO model the average probability $\bar{P}(N_{\max})$ for a coastal hit in the Gulf of Finland within 20 days is 0.62. The similar average value along the optimum fairway is 0.347, giving a gain of 44 % (Soomere et al. 2011c). For the 1 nm OAAS model and 10 days long trajectories $\bar{P} \approx 0.67$ and $p_{\mathrm{opt}} \approx 0.4$ (that is, about 40 % lower) along the optimum fairways shown in Fig. 10.13.

In the same vein the benefit can be expressed in terms of an increase in the time elapsed from the release of the adverse impact until it reaches the coast. The average particle age is 8.7 days in the Gulf of Finland for the 2 nm RCO model and 20-day long trajectories (Soomere et al. 2011c). The average over the points lying on the optimum fairway to the eastern end of the gulf is 12.4 days. The gain is thus up to 42.5 %. The values of a_{opt} and $\bar{A}(N_{\max})$ are much shorter (5.3 and 9 days, respectively) for calculations using 10-day long trajectories and the 1 nm OAAS model (Andrejev et al. 2011).

It is remarkable that the potential in increase in the time available for combating the pollution is almost the same, slightly below 4 days, for radically different model setups. This invariance could suggest that the potential increase in time is largely independent on the particular length of the trajectories (provided the number of hits to the vulnerable area leads to adequate statistics) and possibly is an intrinsic feature of the current-driven dynamics of the particular domain.

The provided statistical estimates of the gain from the systematic use of an optimum sailing line (almost halving the probability for coastal hits or buying almost four days to combat the pollution in the open sea) are obviously considerably overestimated. Such a high benefit is evidently not possible in realistic conditions because a large part of the ship traffic uses anyway deep offshore areas that have relatively low probabilities for coastal hits and high values of the particle age (Andrejev et al. 2011).

10.7.2 Critically Questioning the Recommendations

The computed 2D maps inevitably contain some noise. Given also the intrinsic uncertainties of the technology, it is obvious that the presented solutions are just approximations for the best ones. The above has also shown that they may substantially differ when based on different criteria used in building the maps and may depend on the details and options of the technique. The results for their use in engineering applications, however, have to be robust: new achievements (e.g., an increase in the resolution of the ocean model) may perhaps add more details but should in no way override the principal outcome of the first approximation.

The constructed fairways represent approximations of the climatologically valid solution as they are based on a multi-year average of the underlying fields of probability and particle age from which the potential seasonal effects evidently have been filtered out. Substantial seasonal variations in net and bulk transport patterns calculated using a similar technology (Soomere et al. 2011d), similar variations in the basin-average values of wind stress (Andrejev et al. 2011), significant seasonal patterns of the predominant wind direction (Soomere and Keevallik 2003) and distributions of upwelling regions (Lehmann and Myrberg 2008) suggest that properties of surface transport (and, consequently, the location of the optimum fairway) apparently show extensive seasonal and possibly also interannual variations in the Gulf of Finland. Some of the variations in the dynamical regimes corresponding to the inflow and outflow conditions in the SW Baltic Sea have been addressed in Lu et al. (2012). A much longer time period has to be covered by simulations in order to establish the presence and extension of the related variations in the optimum solutions.

The quality of the recommendations for the location of stationary activities can be roughly estimated as the level of invariance of (the extrema of) the maps of probability, particle age and $\hat{p}$ with respect to different options (Fig. 10.7). There exists, however, no single measure to characterize the quality of the solutions for the optimum fairway. Technically, the robustness of the outcome of the presented approach can be quantified as the typical root-mean-square deviation (rmsd) between the optimum fairways. The difference between various optimum sailing lines can be interpreted as a measure of the uncertainty of the entire approach (Soomere et al. 2010). Uncertainty has not necessarily a negative meaning here: strictly following the optimum path is not always the best solution as ships do need some freedom

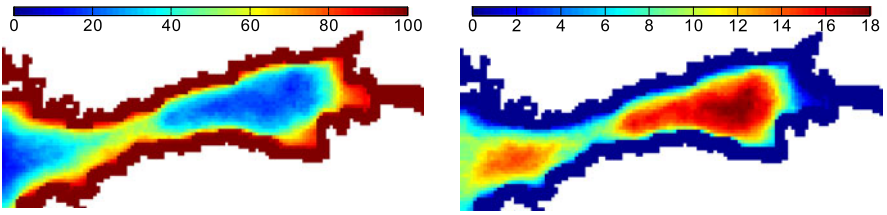

Fig. 10.15 Probabilities (*left panel*, %) of hitting the coast and particle age (*right panel*, days) for the years 1987–1991 calculated with the 2 nm RCO model and TRACMASS code with the time window of 20 days for the Gulf of Finland (Soomere et al. 2011c). Note that the largest values of particle age considerably exceed those calculated in Andrejev et al. (2011) using $t_w = 10$ days

for manoeuvring. For practical purposes it is thus imperative to estimate how sensitive the environmental risks are (e.g., how rapidly the probability increases or the particle age decreases) with respect to small variations in the ships' routes from the theoretical optima.

10.7.3 Robustness and Uncertainty

An attempt to shed light on the questions raised in the previous subsection is described in Soomere et al. (2011c). They used the same ocean model (the 2 nm RCO model), forcing conditions, particle tracking scheme (off-line TRACMASS code), set of 20-day long trajectories of particles released into the centres of each of 3131 sea grid cells in the Gulf of Finland and the 3-cell wide nearshore to consider five different ways to define the optimum fairway. The direct (Method I) and smoothing (II) method were used to specify the equiprobability line as discussed above.

The optimum fairways were calculated using the probability for coastal hits (III) and two methods to handle the age of particles that leave the gulf. Firstly, the age counter was stopped when the particle left the gulf for the first time (IVa). This assumption leads to an obvious underestimation of particle age at the entrance of the gulf (Fig. 10.15). Alternatively, the age for particles leaving the gulf was assigned the length of the time window (IVb). Doing so apparently overestimates particle age for regions of intense water exchange with the Baltic Proper.

The methods basically differ from each other in the definition of the benefit. Only Method I relies on a larger set of trajectories (4 particles in each cell, see above). The optimum fairways were constructed from the extrema or zero-crossing points of the north-south cross-sections of the resulting 2D distributions along 110 discrete longitudes between 21°41′ E and 28°57′ E. The cross-sections of $\hat{p}$ and the resulting fairways based on other measures were smoothed over five subsequent points. The nearshore of all islands in the gulf was ignored and only hits to the mainland coasts were accounted for in order to make the calculations of the equiprobability line and the optimum fairways directly comparable.

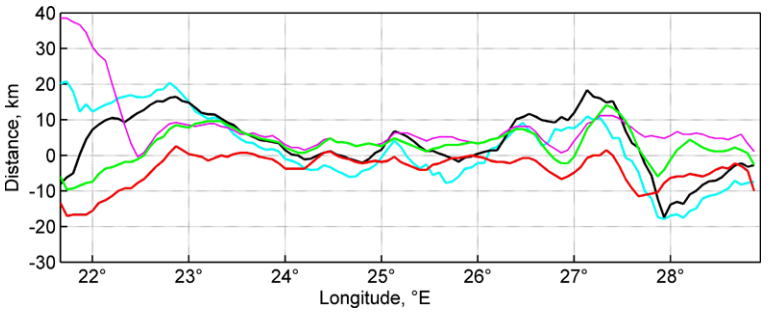

Fig. 10.16 Deviation of the optimum fairways based on Methods I–IV from the centreline of the Gulf of Finland. The positive direction is to the north. The centreline is determined using the 2 nm RCO model grid and not necessarily exactly follows the geographical centreline of the gulf (Soomere et al. 2011c)

The resulting variations in the optimum sailing line implicitly characterize the intrinsic uncertainties (and thus robustness) of the entire approach. The typical rmsd between the optimum fairways specified from different criteria was 6–16 km. This estimate averages out several interesting patterns of the deviations. All five lines were located in a narrow corridor between latitudes 23°40′ E and 26°20′ E where they deviated from each other by <10 km (Fig. 10.16). Such a concentration of the solutions apparently results from the narrowness of this part of the Gulf of Finland where less than ten grid cells represent the offshore dynamics of trajectories and the underlying fields have steep gradients in the north-south direction (Fig. 10.9). The two versions of the equiprobability line were located relatively close to each other (bias 1.6 km, rmsd 6.3 km). The line representing the optimum of the probability of coastal hits follows these lines very closely.

Some of the lines substantially deviated from each other (by up to 50 km) at the entrance to the gulf and in wider parts of this water body where the north–south gradients of the underlying fields were considerably smaller. The systematic deviation of the optimum fairways to the north of the centreline of the gulf (around 27°20′ E) and a smaller deviation to the south around 25°30′ E may be associated with a slow anticyclonic gyre (Soomere et al. 2011d). The large deviation to the south around 28° E evidently reflects the predominant transport to the north in this area jointly by the voluminous runoff of the River Neva and the general cyclonic circulation pattern in the Gulf of Finland (Andrejev et al. 2004a).

Three estimates of optimum fairways out of five were on average located 2–4 km to the north of the centreline of the gulf. Interestingly, the methods IVa and IVb led to quite different locations for the optimum fairway not only at the entrance to the Gulf of Finland but in the entire gulf. The fairway corresponding to Method IVb was located almost 8 km to the north of the axis whereas the one for Method IVa was almost 4 km to the south of the axis (Soomere et al. 2011c). The large deviation of these lines in the entire gulf indicates that particles in the entire northern part of the Gulf of Finland have a large chance to leave the gulf. This example vividly

demonstrates how sensitive the resulting optimum fairway may be with respect to seemingly small variations in the method.

10.7.4 Nearly Optimal Solutions

The issues of robustness and possible uncertainties are closely related to the question of sensitivity of the optimum fairways calculated using different options (Soomere et al. 2011c). A convenient way to quantify the sensitivity of the environmental risks associated with optimum solutions with respect to small variations is to construct a 'corridor' surrounding the optimum sailing line. In such a corridor the underlying measure of risk (probability for a coastal hit, particle age or $\hat{p}$) is allowed to vary to some extent compared to its optimum value. The shape of such corridors together with the values for the gradients of the underlying fields provides information about the flexibility of shipping and characterizes the degree of freedom for captains (or for the decision-making in general) to choose the sailing line with a reasonable increase in the environmental risks. The along-gulf variations in the width of such corridors may also highlight sea regions with different internal dynamics.

The spatial variability of such corridors with a predefined total area (equivalently, with a fixed average width of 15 km in the Gulf of Finland) is analysed in Soomere et al. (2011c) using the 2 nm RCO model, the TRACMASS code and the five specifications of the optimum solution found from the cross-sections of the underlying distributions as described in the previous section. Within such a corridor the probability of coastal hits (or the particle age) is allowed to differ to some extent from the relevant minimum (maximum).

A corridor with an average width of 15 km (8.1 nm) corresponds to an increase in the probability of coastal hits by up to 0.0293 (or to a decrease in the particle age by up to 0.54136 days) for each longitude compared to the optimum value. The corridor's border lines were determined from an analysis of the cross-sections of the underlying distributions as described above. The locations of the probability $p = p_{\min} + 0.293$ ($p_{\min}$ is the minimum probability for the particular longitude) or the particle age of $a = a_{\max} - 0.54136$ days were found for each latitude. The curve consisting of such points was smoothed over five neighbouring points.

The resulting corridors were quite wide at the entrance to the Gulf of Finland, relatively narrow in the Tallinn–Helsinki region (Fig. 10.17), widened substantially in the eastern part of the gulf in the vicinity of Gogland and become very narrow again in the area to the north of Luga Bay. The minimum and maximum widths were 7.35/9.6 km and 29.1/42 km, respectively, for Methods III/IVa.

Similar corridors were defined as the sea area between the equiprobability lines corresponding to $\hat{p} = \pm 0.11189$ for the direct method I and to $\hat{p} = \pm 0.09542$ for the smoothing method II. The fields of $\hat{p}$ had a very steep north–south slope in the central part of the bay in both cases. The corridor for the direct method (Fig. 10.18) had a minimum width of only 2.1 km. The slope was very small at the entrance of the gulf where the resulting corridor was up to 48.6 km wide. The equiprobability line

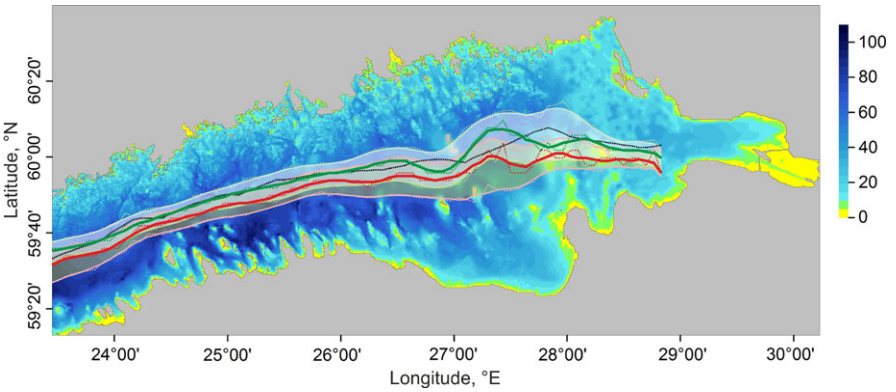

Fig. 10.17 Optimum fairway based on probabilities for coastal hit (*green*) and particle age (*red*, Method IVa) and the relevant 'corridors' with the average width of 15 km in the Gulf of Finland. The *dotted line* shows the geometrical centreline of the gulf (Soomere et al. 2011c). The *background colour scale* shows water depth (m) (Andrejev et al. 2010)

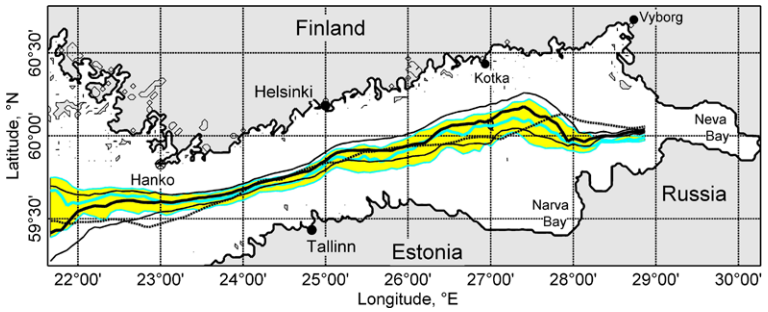

Fig. 10.18 Sea area in which the quantity $\hat{p}$ found using the direct method I is $|\hat{p}| < 0.11189$ (*thin cyan lines* surrounding the *yellow area*) and in which the similar quantity found using the smoothing method II is $|\hat{p}| < 0.09542$ (*thin black lines*) in the Gulf of Finland. *Solid cyan* and *black lines* indicate the relevant equiprobability lines and the *dotted line*—the centreline of the gulf (Soomere et al. 2011c)

was mostly located near to its northern border. The corridor widened up to 26.2 km near Gogland and narrowed considerably at the entrance to the Neva Bay.

The similar corridor for the smoothing method corresponds to $\hat{p} = \pm 0.09542$. It is even narrower (down to 1.19 km) than the one for the direct method in the vicinity of the Tallinn–Helsinki line, reaches a width of over 28 km near Gogland and 37.6 km at the entrance to the Gulf of Finland. Both corridors largely follow the centreline in the narrowest part of the gulf but deviate considerably to the north of it in the vicinity of Gogland. The two equiprobability lines and corridors almost coincide near Hanko (where they are located up to 10 km to the north from the centreline) but deviate from each other in the entrance area of the Gulf of Finland. The drastic variations (from 1 or 2 km up to 30 km) of their local width signify

that the sensitivity of the results with respect to small changes in the environmental criteria may largely vary in different parts of the gulf (Soomere et al. 2011c).

10.7.5 Limitations of Modelling

The construction of different maps using the presented technology and specifically studies of its reliability and associated uncertainties are computationally expensive and time-consuming. It is thus natural to address potential simplifications of the calculations involving a minimum loss of accuracy but retaining the reliability of the results. A generic way of reducing the computational efforts is to decrease the resolution of the underlying hydrodynamic model. Doing so is only feasible until the model still adequately reproduces the mesoscale dynamics (cf. Albretsen and Røed 2010). As computational costs increase rapidly when increasing the 3D model resolution, such a reduction is still highly desired for the practical use of the technique. A natural limit is that the model should be at least eddy-permitting. This is a severe condition in the test areas of the Baltic Sea where the baroclinic Rossby radius is usually about 2–4 km, and may be even down to 0.5–1 km at specific locations (Fennel et al. 1991; Osiński et al. 2010; Nekrasov and Lebedeva 2002).

Experience from numerical physical oceanography suggests that although the instantaneous simulated currents are quite different for different resolutions and even the statistics of currents may exhibit substantial changes for different model resolutions (Albretsen and Røed 2010), some other fields such as salinity or temperature can be reasonably replicated using models that poorly resolve the mesoscale dynamics. Moreover, these fields may remain practically the same at different resolutions (Andrejev et al. 2010; Myrberg et al. 2010b). For example, the appearance of simulated currents in the Gulf of Finland may change abruptly when the resolution is increased from 0.5 to 0.25 nm but the salinity and temperature fields are almost the same as for a resolution of 1 nm (Andrejev et al. 2010).

The overall location of the lowest probabilities of coastal hits in the meridional cross-sections generally corresponds to the location of the equiprobability lines in the western and central parts of the gulf in 2 nm simulations that ignored the presence of islands. The increase in the resolution from 2 nm to 1 nm and/or the more exact representation of islands leads to several obvious differences in the results for the eastern part of the gulf, especially between Gogland and Kotka (cf. Fig. 10.7 and Fig. 10.14). In this context, it is natural to ask whether the above-mentioned maps of environmental risks (reflecting, in essence, long-term statistics of the current-driven transport), or at least certain parts of their integral features, belong to the family of those characteristics that are largely insensitive to changes in the resolution of the underlying ocean model. A related task is to identify an optimum spatial resolution for the ocean model for different applications in a particular basin.

10.7.6 Sensitivity to the Resolution of the Ocean Model

The sensitivity of the technology in this respect is analysed in Andrejev et al. (2011) based on on-line simulations of 10-day long Lagrangian trajectories calculated for the period of 1 May 1987–31 December 1991 for the Gulf of Finland. The relevant maps for the probability of coastal hits and for the particle age are evaluated using the OAAS model at three different horizontal resolutions of 2, 1 and 0.5 nm and with otherwise identical vertical resolution, initial, boundary and forcing conditions, and trajectory calculation scheme. This range of resolutions characterizes a transition from a poor representation of mesoscale effects by an eddy-permitting model to one which is expected to adequately resolve statistical features of the field of mesoscale eddies.

The dynamics of water masses in the Gulf of Finland is extremely complicated and the resolution of even the 0.5 nm model does not perfectly resolve all the small-scale features of water motion. The impact of subgrid-scale turbulence on the spreading of trajectories was parameterized by the addition of a random disturbance containing a strong rotational component as described above. The resulting set of 2D maps of cell-wise probability of hitting the coast and particle age is presented in Fig. 10.7. The general appearance of the distributions for the probabilities and particle age are fairly similar in different resolutions. Particularly close are the fields for 1 nm and 0.5 nm resolutions. The correlation between pointwise values of probability and particle age is 0.98, the bias for p is 0.024 and for age as low as 0.012. The mean absolute deviation is 0.037 and 0.21, respectively. The rmsd between the two sets of fields is even smaller, 0.0021 and 0.081, respectively.

Also several integral measures almost coincide for the three resolutions. The spatially averaged limiting values of the probability $\bar{P}(N_{\max})$ and the particle age $\bar{A}(N_{\max})$ also display hardly any dependence on the resolution. They both reach almost identical stationary levels (0.66–0.69 and 5.25–5.33 days, respectively; the standard deviations vary from 0.16 to 0.19 and 1.06 to 1.30) after five years of simulations (Andrejev et al. 2011).

The resulting solutions for fairways may be much more strongly affected by the particular horizontal resolution of the ocean model than the integral variables and 2D maps discussed above. In spite of the almost perfect match of the integral characteristics the optimum fairways only match each other in certain parts of the gulf (Fig. 10.19). They only overlap in a short section of the narrowest part of the gulf between Naissaar and Porkkala and converge at a certain point to the north of Lahemaa. The fairways for the 1 nm and 0.5 nm resolutions also converge in the narrow passages between the islands to the south of Gogland (Soomere et al. 2011b, 2011c).

In other parts of the gulf the optimum fairways calculated using different resolutions show a complicated pattern of behaviour. While all the optimum lines are concentrated into a narrow corridor to the west of Naissaar, they deviate considerably from each other even in the narrow area between Tallinn and Helsinki. The fairways to Vyborg calculated at different resolutions visit completely different areas of the Gulf of Finland (Fig. 10.18). While the differences between the fairways at the 1 nm and 0.5 nm resolutions are moderate, the fairway for the 2 nm model

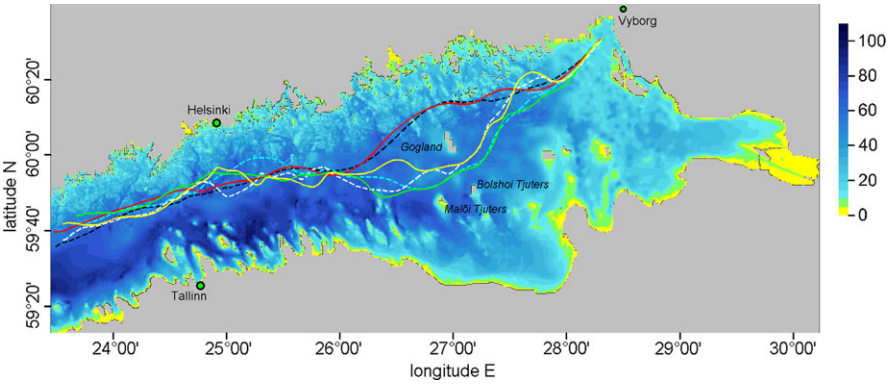

Fig. 10.19 Optimum fairways to Vyborg according to the spatial distributions of the probability for coastal hits (*solid lines*) and the particle age (*dashed lines*) at resolutions of 2 nm (*red* and *black* respectively), 1 nm (*green* and *cyan*) and 0.5 nm (*yellow* and *white*). The depth scale to the right of the map is given in metres (Andrejev et al. 2011)

apparently reflects a completely different pattern of underlying dynamics, especially in the central part of the Gulf of Finland.

This example vividly illustrates the importance of the choice of an adequate horizontal resolution on the resulting location of the optimum fairway. Although the spatial distributions of the relevant fields are qualitatively similar for all resolutions, the optimum locations for fairways depend substantially on the resolution. It is remarkable that the results for the 2 nm model differ considerably from those obtained using finer-resolution models. As mentioned above, it is not possible to judge on the basis of our simulations whether or not this difference is driven by the accuracy of simulations of hydrodynamics and/or whether the accuracy of the representation of the Finnish archipelago plays a role.

Interestingly, the potential benefit from the use of the optimum fairway (estimated, e.g., as the difference between the mean probability of coastal hits and the average value of this probability along the optimum fairway) very little depends on the resolution of the ocean model. The benefit is also not directly connected with the length of the resulting fairway. The longest of the three optima in Fig. 10.19 offers the largest benefit. It leads to a decrease in the relevant probability from the mean value of 0.67 to 0.46 along the fairway (Andrejev et al. 2011). Somewhat surprisingly, the best formal benefit (mean probability over the optimum fairway 0.432) is provided by the 2 nm model. The highest-resolution model provides a fairway with the mean probability of 0.536 and with a very modest gain.

10.8 Concluding Remarks

The proposed technique combines several advanced applications (a 3D circulation model, a Lagrangian trajectory tracking method, a statistical analysis of certain

probabilities, and a method for 2D optimization) into one entity. Although construction of a single modelling system is possible, we have intentionally highlighted the interfaces and connections between the separate basic steps so that the user may easily replace each component with a more convenient or more elaborated one. The essence of the method does not depend on the properties of a particular model for each single step. The presented approaches highlight the potential of such a multi-step modelling system for the preventive planning of maritime activities. They also reveal several instructive features of the outcome of the technique and particularly the importance of a feasible choice of the target function.

It is important to emphasize that implementations of the technology described in this chapter are based on several simplifications, and the validity of some of them is not obvious. They mostly account for the impact of surface-current-driven propagation of pollution on the optimum solution. Realistic applications have to account for not only the impact of wave- and wind-induced transport of contaminants but also complicated physical and chemical processes affecting their fate (ASCE 1996). These questions will be partially addressed in Chap. 11.

The constructed example fairways are only conditionally optimized. The presented idealized examples (in which only the current-driven propagation is accounted for) signify, however, that the impact of current-driven transport may add a significant contribution to the marine-induced hazards in certain coastal sections. A major simplification that might not be entirely justified is neglecting the potential impact of subgrid-scale processes in applications using the RCO model and the DMI/BSHcmod model. Doing so may considerably alter the statistics of trajectories, especially for longer time intervals.

The presented material suggests that eddy-permitting models with a grid step exceeding half the local baroclinic Rossby radius are suitable for a quick check of whether or not any potential gain from the presented method is feasible. However, higher-resolution simulations using eddy-resolving models are definitely necessary for detailed planning.

Although the instantaneous values of the basin-wide probability of coastal hits and particle age reveal substantial spatio-temporal variations in different sea areas and/or in different years and seasons (Fig. 10.3), their cumulative values converge quite rapidly to a fixed level for a wide range of resolutions of the ocean model. This convergence suggests that these asymptotic values characterize certain intrinsic combinations of the geometry of the basin and internal current structure, and perhaps even could be interpreted as new measures of the vulnerability of the nearshore of water bodies to offshore traffic accidents for the chosen length of time window. The (spatial) standard deviation of the probability and particle age indicates the magnitude of their variations across the water body and thus serves as a natural indicator implicitly characterizing the potential benefit from the smart positioning of dangerous activities for the particular sea area.

The very limited dependence of several discussed measures and properties on the resolution of the underlying hydrodynamic models needs some attention. The probable reason is the multi-step averaging procedure of short-term transport features (over time intervals exceeding the typical turnover time of mesoscale eddies

and over the 5-year time interval) that filters out many short-term features of the circulation. This filtering apparently affects the results of simulations that satisfactorily capture the mesoscale features to an almost equal extent. The overall match of the optimum fairways for the 1 nm and 0.5 nm models suggests that the decisive aspects of the mesoscale circulation of the Gulf of Finland (Andrejev et al. 2004a), including the combined effects of the prevailing SW winds, the general structure of the density field, the bathymetry and geometry of the gulf, etc., have been adequately obtained using the 1 nm OAAS model. In other words, one might speculate that the 1 nm model reproduces the statistical properties of current-driven transport in the Gulf of Finland quite well. This conjecture is not completely unexpected but is nevertheless interesting.

Acknowledgements This study was supported by the funding from the Estonian Science Foundation and the European Community's Seventh Framework Programme (2007–2013) under grant agreement No. 217246 made with the joint Baltic Sea research and development programme BONUS. The BalticWay project attempted to identify the regions in the Baltic Sea that are associated with increased risk compared to other sea areas and to propose ways to reduce the risk of them being polluted by placing activities in other areas that may provide less risk. The research was also partially supported by the Marie Curie RTN SEAMOCS (MRTN-CT-2005-019374), the Marie Curie Transfer of Knowledge project CENS-CMA (MC-TK-013909), Marie Curie Reintegration Grant ESTSpline (PERG02-GA-2007-224819), the targeted financing by the Estonian Ministry of Education and Science (grants SF0140077s08 and SF0140007s14) and the Estonian Science Foundation (grant No. 7413). The contribution of Anders Anbo towards the application of the TRACMASS model in the Institute of Cybernetics and the help from Kristofer Döös during its use are gratefully acknowledged. The Wave Engineering Laboratory team is deeply grateful to Markus Meier and Anders Höglund (SMHI) who provided the RCO model data and meteorological forcing in the framework of the BONUS cooperation.

References

Abascal AJ, Castanedo S, Medina R, Liste M (2010) Analysis of the reliability of a statistical oil spill response model. Mar Pollut Bull 60:2099–2110

Albretsen J, Røed LP (2010) Decadal simulations of mesoscale structures in the northern North Sea/Skagerrak using two ocean models. Ocean Dyn 60:933–955

Alenius P, Myrberg K, Nekrasov A (1998) Physical oceanography of the Gulf of Finland: a review. Boreal Environ Res 3:97–125

Alenius P, Nekrasov A, Myrberg K (2003) The baroclinic Rossby-radius in the Gulf of Finland. Cont Shelf Res 23:563–573

Ambjörn C (2007) Seatrack web, forecasts of oil spills, a new version. Environ Res Eng Manag 3(41):60–66

Ambjörn C (2008) Seatrack web forecasts and backtracking of oil spills—an efficient tool to find illegal spills using AIS. In: IEEE/OES US/EU-Baltic international symposium, Tallinn, Estonia, May 27–29, 2008. IEEE Press, New York, pp 168–176

Andrejev O, Sokolov A (1989) Numerical modelling of the water dynamics and passive pollutant transport in the Neva inlet. Meteorol Hydrol 12:75–85 (in Russian)

Andrejev O, Sokolov A (1990) 3D baroclinic hydrodynamic model and its applications to Skagerrak circulation modelling. In: Proc 17th conf Baltic oceanographers, Norrköping, Sweden, pp 38–46

Andrejev O, Myrberg K, Alenius P, Lundberg PA (2004a) Mean circulation and water exchange in the Gulf of Finland—a study based on three-dimensional modelling. Boreal Environ Res 9:1–16

Andrejev O, Myrberg K, Lundberg PA (2004b) Age and renewal time of water masses in a semi-enclosed basin—application to the Gulf of Finland. Tellus A 56:548–558

Andrejev O, Sokolov A, Soomere T, Värv R, Viikmäe B (2010) The use of high-resolution bathymetry for circulation modelling in the Gulf of Finland. Est J Eng 16:187–210

Andrejev O, Soomere T, Sokolov A, Myrberg K (2011) The role of spatial resolution of a three-dimensional hydrodynamic model for marine transport risk assessment. Oceanologia 53:309–334

ASCE Task Committee on modeling of oil spills, Water Resources Engineering Division [ASCE] (1996) State-of-the-art review of modeling transport and fate of oil spills. J Hydraul Eng 122:594–609

Bergström S, Carlsson B (1994) River runoff to the Baltic Sea: 1950–1990. Ambio 23:280–287

Blanke B, Raynard S (1997) Kinematics of the Pacific Equatorial Undercurrent: an Eulerian and Lagangian approach from GCM results. J Phys Oceanogr 27:1038–1053

Blumberg A, Mellor G (1987) A description of a three-dimensional coastal ocean circulation model. In: Heaps NS (ed) Three-dimensional Coastal Ocean models. Coastal and estuarine science series, vol 4. American Geophysical Union, Washington, DC, pp 1–16

Bowden-Kerby A (2001) The original MPAs (Marine protected areas). MPA News 3:5–6

de Vries P, Döös K (2001) Calculating Lagrangian trajectories using time-dependent velocity fields. J Atmos Ocean Technol 18:1092–1101

Deleersnijder E, Campin J-M, Delhez EJM (2001) The concept of age in marine modelling. I. Theory and preliminary model results. J Mar Syst 28:229–267

Delpeche-Ellmann NC, Soomere T (2013) Investigating the Marine Protected Areas most at risk of current-driven pollution in the Gulf of Finland, the Baltic Sea, using a Lagrangian transport model. Mar Pollut Bull 67:121–129

Dick S, Kleine E, Müller-Navarra S (2001) The operational circulation model of BSH (BSH cmod). Model description and validation. Berichte des Bundesamtes für Seeschifffahrt und Hydrographie 29/2001. Hamburg, Germany, 48 pp

Döös K (1995) Inter-ocean exchange of water masses. J Geophys Res—Oceans 100:13,499–13,514

Döös K, Engqvist A (2007) Assessment of water exchange between a discharge region and the open sea—a comparison of different methodological concepts. Estuar Coast Shelf Sci 74:585–597

Döös K, Nycander J, Coward AC (2008) Lagrangian decomposition of the Deacon Cell. J Geophys Res—Oceans 113:C07028

Drijfhout SS (1989) Eddy-genesis and the related heat transport: a parameter study. In: Nihoul JCJ, Jamart BM (eds) Mesoscale/synoptic coherent structures in geophysical turbulence. Elsevier oceanography series, vol 50, pp 245–263

Eide MS, Endresen Ø, Brett PE, Ervik JL, Røang K (2007) Intelligent ship traffic monitoring for oil spill prevention: risk based decision support building on AIS. Mar Pollut Bull 54:145–148

Elken J, Raudsepp U, Lips U (2003) On the estuarine transport reversal in deep layers of the Gulf of Finland. J Sea Res 49:267–274

Engqvist A, Andrejev O (2003) Water exchange of the Stockholm archipelago—a cascade framework modelling approach. J Sea Res 49:275–294

Engqvist A, Döös K, Andrejev O (2006) Modeling water exchange and contaminant transport through a Baltic coastal region. Ambio 35:435–447

Fennel W, Seifert T, Kayser B (1991) Rossby radii and phase speeds in the Baltic Sea. Cont Shelf Res 11:23–36

French DP, Rines H, Masciangioli P (1997) Validation of an orimulsion spill fates model using observations from field test spill. In: Proceedings of the 20th Arctic and Marine oil spill program (AMOP) technical seminar, environment, Canada, Ottawa, Ontario, pp 933–961

French-McCay DP (2004) Oil spill impact modeling: development and validation. Environ Toxicol Chem 23:2441–2456
Funkquist L (2001) HIROMB: an operational eddy-resolving model for the Baltic Sea. Bull Mar Inst, Gdańsk 28:7–16
Gästgifvars M, Lauri H, Sarkanen A-K, Myrberg K, Andrejev O, Ambjörn C (2006) Modelling surface drifting of buoys during a rapidly-moving weather front in the Gulf of Finland, Baltic Sea. Estuar Coast Shelf Sci 70:567–576
Glasby GP (1997) Disposal of chemical weapons in the Baltic Sea. Sci Total Environ 208:145–147
Gollasch S, Leppäkoski E (2007) Risk assessment and management scenarios for ballast water mediated species introduction into the Baltic Sea. Aquat Invasions 2:313–340
Gray JS (1997) Marine biodiversity: patterns, threats and conservation needs. Biodivers Conserv 6:153–175
Gräwe U, Wolff J-O (2010) Suspended particulate matter dynamics in a particle framework. Environ Fluid Mech 10:21–39
Griffa A, Piterbarg LI, Özgökmen T (2004) Predictability of Lagrangian particle trajectories: effects of smoothing of the underlying Eulerian flow. J Mar Res 62:1–35
HELCOM (2009) In: Stankiewicz M, Vlasov N (eds) Ensuring safe shipping in the Baltic. Helsinki Commission, Helsinki, 18 pp
Höglund A, Meier HEM (2012) Environmentally safe areas and routes in the Baltic Proper using Eulerian tracers. Mar Pollut Bull 64:1375–1385
Höglund A, Meier HEM, Broman B, Kriezi E (2009) Validation and correction of regionalised ERA-40 wind fields over the Baltic Sea using the Rossby Centre Atmosphere Model RCA3.0. Rapport Oceanografi No 97, Swedish Meteorological and Hydrological Institute, Norrköping, Sweden, 29 pp
Jönsson B, Lundberg P, Döös K (2004) Baltic sub-basin turnover times examined using the Rossby Centre Ocean model. Ambio 23:257–260
Kachel MJ (2008) Particularly sensitive sea areas. Hamburg studies on Maritime Affairs, vol 13. Springer, Berlin, pp 376
Kleine E (1994) Das operationelle Modell des BSH für Nordsee und Ostsee. Bundesamt für Seeschifffart und Hydrographie, 126 pp (in German)
Kokkonen T, Ihaksi T, Jolma A, Kuikka S (2010) Dynamic mapping of nature values to support prioritization of coastal oil combating. Environ Model Softw 25:248–257
Kurennoy D, Parnell KE, Soomere T (2011) Fast-ferry generated waves in South-West Tallinn Bay. J Coast Res 64(Special Issue):165–169
Lehmann A (1995) A three-dimensional baroclinic eddy-resolving model of the Baltic Sea. Tellus A 47:1013–1031
Lehmann A, Myrberg K (2008) Upwelling in the Baltic Sea—a review. J Mar Syst 74:S3–S12
Lehmann A, Krauss W, Hinrichsen H-H (2002) Effects of remote and local atmospheric forcing on circulation and upwelling in the Baltic Sea. Tellus A 54:299–316
Lekien F, Coulliette C, Marsden J (2003) Lagrangian structures in very high-frequency radar data and optimal pollution timing. In: Experimental chaos. AIP conference proceedings, vol 676, pp 162–168
Leppäranta M, Myrberg K (2009) Physical oceanography of the Baltic Sea. Springer Praxis, Berlin, 378 pp
Lessin G, Ossipova V, Lips I, Raudsepp U (2009) Identification of the coastal zone of the central and eastern Gulf of Finland by numerical modeling, measurements, and remote sensing of chlorophyll *a*. Hydrobiologia 692:187–198
Lidskog R, Elander I (2012) Sweden and the Baltic Sea pipeline: between ecology and economy. Mar Policy 36:333–338
Lilover M-J, Pavelson J, Kõuts T (2011) Wind forced currents over the shallow Naissaar Bank in the Gulf of Finland. Boreal Environ Res 16(Suppl A):164–174
Lindow H (1997) Experimentelle Simulationen windangeregter dynamischer Muster in hochauflösenden numerischen Modellen. Meereswissenschaftliche Berichte No 22, Institut für Ostseeforschung, Warnemünde (in German)

Liu S-K, Leendertse J (1978) Multidimensional numerical modelling of estuaries and coastal seas. Adv Hydrosci 11:95–164
Lu X, Soomere T, Stanev EV, Murawski J (2012) Identification of the environmentally safe fairway in the South-Western Baltic Sea and Kattegat. Ocean Dyn 62:815–829
Matthäus W, Lass HU (1995) The recent salt inflow into the Baltic Sea. J Phys Oceanogr 25:280–286
Meier HEM (2001) On the parameterization of mixing in three-dimensional Baltic Sea models. J Geophys Res—Oceans 106:30,997–31,016
Meier HEM (2007) Modeling the pathways and ages of inflowing salt- and freshwater in the Baltic Sea. Estuar Coast Shelf Sci 74:610–627
Meier HEM, Döscher R, Faxén T (2003) A multiprocessor coupled ice-ocean model for the Baltic Sea: application to salt inflow. J Geophys Res—Oceans 108:3273
Mesinger F, Arakawa A (1976) Numerical methods used in atmospheric models. GARP publications series 17, vol I. WMO, Geneva, 64 pp
Millero F, Kremling I (1976) The densities of the Baltic Sea deep waters. Deep-Sea Res 23:611–622
Myrberg K, Andrejev O (2003) Main upwelling regions in the Baltic Sea—a statistical analysis based on three-dimensional modelling. Boreal Environ Res 8:97–112
Myrberg K, Andrejev O, Lehmann A (2010a) Dynamic features of successive upwelling events in the Baltic Sea—a numerical case study. Oceanologia 52:77–99
Myrberg K, Ryabchenko V, Isaev A, Vankevich R, Andrejev O, Bendtsen J, Erichsen A, Funkquist L, Inkala A, Neelov I, Rasmus K, Rodriguez Medina M, Raudsepp U, Passenko J, Söderkvist J, Sokolov A, Kuosa H, Anderson TR, Lehmann A, Skogen MD (2010b) Validation of three-dimensional hydrodynamic models in the Gulf of Finland based on a statistical analysis of a six-model ensemble. Boreal Environ Res 15:453–479
Nekrasov AV, Lebedeva IK (2002) Estimation of baroclinic Rossby radii in Luga-Koporye region. BFU Res Bull 4(5):89–93
Ollitrault M, Gabillet C, Colin de Verdiere A (2005) Open ocean regimes of relative dispersion. J Fluid Mech 533:381–407
Osiński R, Piechura J (2009) Latest findings about circulation of upper layer in the Baltic Proper. In: BSSC 2009 abstract book, Tallinn, August 17–21, 2009, p 103
Osiński R, Rak D, Walczowski W, Piechura J (2010) Baroclinic Rossby radius of deformation in the southern Baltic Sea. Oceanologia 52:417–429
Parnell KE, Delpeche N, Didenkulova I, Dolphin T, Erm A, Kask A, Kelpšaitė L, Kurennoy D, Quak E, Räämet A, Soomere T, Terentjeva A, Torsvik T, Zaitseva-Pärnaste I (2008) Far-field vessel wakes in Tallinn Bay. Est J Eng 14:273–302
Reed M, Johansen O, Brandvik PJ, Daling P, Lewis A, Fiocco R, Mackay D, Prentki R (1999) Oil spill modeling towards the close of the 20th century: overview of the state of the art. Spill Sci Technol Bull 5:3–16
Rice J (2003) Environmental health indicators. Ocean Coast Manag 46:235–259
Richardson LF (1926) Atmospheric diffusion shown on a distance-neighbour graph. Proc R Soc A 110:709–737
Samuelsson P, Jones CG, Willén U, Ullerstig A, Gollvik S, Hansson U, Jansson C, Kjellström E, Nikulin G, Wyser K (2011) The Rossby Centre Regional Climate model RCA3: model description and performance. Tellus A 63:4–23
Seifert T, Tauber F, Kayser B (2001) A high resolution spherical grid topography of the Baltic Sea, 2nd edition. In: Baltic Sea Science Congress, Stockholm, 25–29 November 2001. Poster #147. www.io-warnemuende.de/iowtopo
Sokolov A, Andrejev O, Wulff F, Rodriguez Medina M (1997) The data asssimilation system for data analysis in the Baltic Sea. System Ecology Contributions No 3. Stockholm University, Sweden, 66 pp
Soomere T, Keevallik S (2003) Directional and extreme wind properties in the Gulf of Finland. Proc Est Acad Sci, Eng 9:73–90

Soomere T, Quak E (2007) On the potential of reducing coastal pollution by a proper choice of the fairway. J Coast Res 50(Special Issue):678–682
Soomere T, Viikmäe B, Delpeche N, Myrberg K (2010) Towards identification of areas of reduced risk in the Gulf of Finland, the Baltic Sea. Proc Est Acad Sci 59:156–165
Soomere T, Andrejev O, Sokolov A, Myrberg K (2011a) The use of Lagrangian trajectories for identification the environmentally safe fairway. Mar Pollut Bull 62:1410–1420
Soomere T, Andrejev O, Sokolov A, Quak E (2011b) Management of coastal pollution by means of smart placement of human activities. J Coast Res 64(Special Issue):951–955
Soomere T, Berezovski M, Quak E, Viikmäe B (2011c) Modeling environmentally friendly fairways in elongated basins using Lagrangian trajectories: a case study for the Gulf of Finland, the Baltic Sea. Ocean Dyn 61:1669–1680
Soomere T, Delpeche N, Viikmäe B, Quak E, Meier HEM, Döös K (2011d) Patterns of current-induced transport in the surface layer of the gulf of Finland. Boreal Environ Res 16(Suppl A):49–63
Soomere T, Viidebaum M, Kalda J (2011e) On dispersion properties of surface motions in the Gulf of Finland. Proc Est Acad Sci 60:269–279
Stokstad E (2009) US poised to adopt national ocean policy. Science 326:1618
Vandenbulcke L, Beckers J-M, Lenartz F, Barth A, Poulain P-M, Aidonidis M, Meyrat J, Ardhuin F, Tonani M, Fratianni C, Torrisi L, Pallela D, Chiggiato J, Tudor M, Book JW, Martin P, Peggion G, Rixen M (2009) Super-ensemble techniques: application to surface drift prediction. Prog Oceanogr 82:149–167
Viikmäe B, Soomere T (2013) Spatial pattern of hits to the nearshore from a major marine highway in the Gulf of Finland. J Mar Syst
Viikmäe B, Soomere T, Viidebaum M, Berezovski A (2010) Temporal scales for transport patterns in the Gulf of Finland. Est J Eng 16:211–227
Viikmäe B, Soomere T, Parnell KE, Delpeche N (2011) Spatial planning of shipping and offshore activities in the Baltic Sea using Lagrangian trajectories. J Coast Res 64(Special Issue):956–960
Webb DJ, Coward AC, de Cuevas BA, Gwilliam CS (1997) A multiprocessor ocean circulation model using message passing. J Atmos Ocean Technol 14:175–183
WWF (2010) Future trends in the Baltic Sea. WWF Baltic Ecoregion Programme. Solna, Sweden, 40 pp
Zhurbas V, Laanemets J, Vahtera E (2008) Modeling of the mesoscale structure of coupled upwelling/downwelling events and the related input of nutrients to the upper mixed layer in the Gulf of Finland, Baltic Sea. J Geophys Res—Oceans 113:C05004

http://www.springer.com/978-3-319-00439-6

Preventive Methods for Coastal Protection
Towards the Use of Ocean Dynamics for Pollution Control
Soomere, T.; Quak, E. (Eds.)
2013, XVIII, 442 p. 171 illus., 138 illus. in color.,
Hardcover
ISBN: 978-3-319-00439-6